Universidade de Aveiro Departamento de Química
2014

Marta Julia Busse

Bionanocompositos de Fe_3O_4/SiO_2 e alginato para remoção magnética de espécies de Cr(III) em água

Bionanocomposites of Fe_3O_4/SiO_2 and alginate for magnetic removal of Cr(III) species from water

Universidade de Aveiro Departamento de Química
2014

Marta Julia Busse

Bionanocompositos de Fe_3O_4/SiO_2 e alginato para remoção magnética de espécies de Cr(III) em água

Bionanocomposites of Fe_3O_4/SiO_2 and alginate for magnetic removal of Cr(III) species from water

dissertação apresentada à Universidade de Aveiro para cumprimento dos requisitos necessários à obtenção do grau de Mestre em Química,realizada sob a orientação científica do Proffesor Doutor Tito da Silva Trindade, Professor Associado do Departamento de Química da Universidade de Aveiro e Doutora Ana Luísa Daniel da Silva, Investigadora Auxiliar do Departamento de Química da Universidade de Aveiro

o júri

presidente

Prof. Doutor Artur Manuel Soares da Silva
Professor Catedrático do Departamento de Qumíca da Universidade de Aveiro

Prof. Doutora Olinda Coelho Monteiro
Professora Auxiliar Convidada da Faculdade de Ciências da Universidade de Lisboa

Doutora Ana Luísa Daniel da Silva
Investigadora Auxiliar do Departamento de Química da Universidade de Aveiro

agradecimentos

I would like to thank Professor Tito da Silva Trindade, Doctor Ana Luísa Daniel da Silva and Professor Wojciech Kinart for help me to prepare this thesis and I would like to thank to C (undação para a Ciência e a Tecnologia) for funding this work through the project PTDC/CTM-NAN/120668/2010, FEDER through COMPETE and by national funding through FCT in the frame of project CICECO-FCOMP-01-0124-FEDER-037271 (Ref. FCT Pest-C/CTM/LA0011/2013). Also I would like to thank to Dra. Teresa Caldeira (University of Aveiro) for AAS measurements.

Palavras-chave Nanopartículas magnéticas, alginato, remoção de poluentes, Cr (III).

resumo

O objectivo do presente trabalho foi o de estudar a eliminação de Cr (III), a partir de soluções aquosas, por processo de adsorção, utilizando nanopartículas magnéticas funcionalizadas com grupos amina e com o polissacarídeo alginato.

A poluição causada por metais pesados está na base de graves problemas de saúde pública e ambientais em todo o mundo. O crómio é um dos metais mais tóxicos, pondo em perigo a vida humana. O Cr (III) é frequentemente usado na indústria, causando a poluição da água. Por esta razão, aumentou o interesse dos investigadores na utilização de nanomateriais para a remoção de poluentes e no estudo de adsorventes para substituir materiais caros, nomeadamente matérias-primas de baixo custo, tais como, materiais provenientes de polímeros residuais ou subprodutos agrícolas.

Este trabalho incluiu a preparação de nanopartículas magnéticas, o seu revestimento com uma capa de sílica amorfa funcionalizada com grupos de amina e a ligação covalente do alginato à nanopartícula magnética. As propriedades das nanopartículas foram avaliadas utilizando várias técnicas experimentais nomeadamente difracção de raios-X, espectroscopia de infravermelho, análise elementar, termogravimetria e medições do potencial zeta.

As nanopartículas magnéticas revestidas com sílica e funcionalizadas com grupos de amina foram investigadas para a adsorção de Cr (III) / complexos de EDTA de águas, enquanto que as nanopartículas ligadas às moléculas de alginato foram testadas para a remoção de iões Cr (III) em meio aquoso. Os resultados de cinética foram ajustados aos modelos de pseudo-primeira e pseudo-segunda ordem, e os resultados de equilíbrio de adsorção foram ajustados aos modelos adequados, tais como a isotérmica de Langmuir e a de Freundlich.

As nanopartículas compósitas revelaram ter afinidade para as espécies de Cr (III). Devido às suas propriedades, estas nova nanopartículas compósitas podem encontrar aplicações interessantes na purificação de águas.

keywords Magnetic nanoparticles, alginate, pollutant removal, Cr (III).

abstract

The aim of the present work was to study the removal of Cr (III) species from aqueous solutions by adsorption process, using magnetic nanoparticles functionalized with amine groups and with the polysaccharide alginate.

Heavy metal pollution is serious environmental and public health problem worldwide. Chromium is one of the most toxic metal endangering human life. Cr(III) is often used in industry which caused water pollution. Therefore, increased interest by the researchers to employ nanomaterials for the removal contamination and explore adsorbents to replace expensive materials, particularly low-cost raw materials such as, residual polymers materials or agricultural by-products.

The work included the preparation of magnetic nanoparticles, coating them with amorphous silica shell functionalized with amine groups and the covalent attachment of alginate to the magnetic nanoparticle. The properties of the nanoparticles were assessed by a number of experimental techniques namely x-ray diffraction, infrared spectroscopy, elemental analysis, thermogravimetry and zeta potential measurements.

Silica coated magnetic nanoparticles functionalized with amine groups were investigated for the uptake of Cr(III)/EDTA complexes from water, while the nanoparticles attached to the alginate molecules were tested for the removal of aqueous Cr(III) ions. The kinetic results were fitted to models of pseudo first and pseudo second order and the equilibrium adsorption results were adjusted to suitable isotherm models such as Langmuir and Freundlich.

The composite nanoparticles revealed affinity to the Cr(III) species. Due to its properties, this new composite nanoparticles may find interesting applications in purification of water.

Contents

Abbreviations

AAS	atomic absorption spectrometry
ALD	alginate
APTES	3-aminopropyltriethoxysilane
APTMS	3-aminopropyltrimethoxysilane
DLS	Dynamic Light Scattering
DMSA	dimercaptosuccinic
EDC	N-(3-dimethylaminopropyl)-N'-ethylcarbodiimide hydrochloride
EDTA-Na_2	ethylenediaminetetraacetic acid
FTIR	Fourier Transform Infrared spectroscopy
HA	humic acid
NHS	N-hydroxysuccinimide
ODS	octadecylsilane
SA	Salicylic acid
SEM	Scanning Electron Microscopy
TEM	Transmission Electron Microscopy
TEOS	tetraethyl orthosilicate
TGA	Thermogravimetric Analysis
TGA	thermogravimetric analysis
UV-VIS	Ultraviolet-Visible
XRD	Powder X-ray Diffraction
Cr(HY)(H_2O)	chromium(III) complex with EDTA

List of figures and tables

Figures

Tables

1. Introduction

In the past decade nanomaterials have gained increasing attention for scientists and engineers, because of their special properties. Size effects and increased fraction of "surface" atoms result in the change of chemical and physical properties of there small particles [1]. Typically, nanomaterials have at least one dimension between 1 and 100 nm [2].

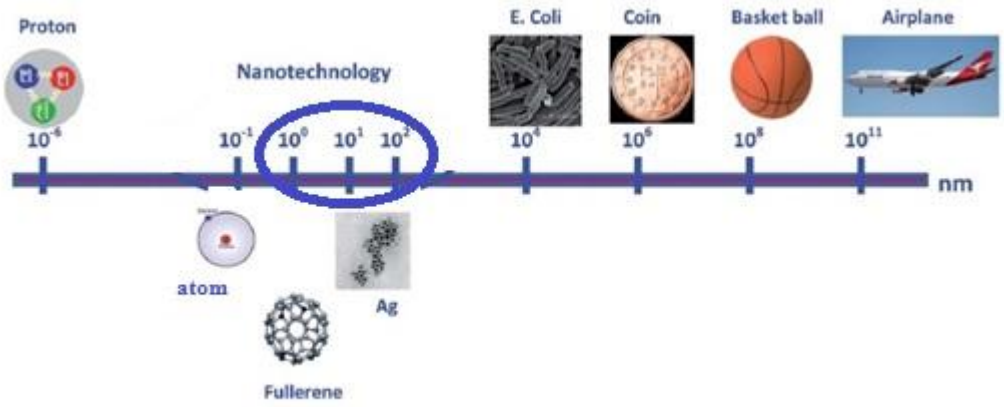

Figure 1. Comparative sizes of various entities to perceive nanoscale measurements [2].

The unique physical and chemical properties of nanomaterials lead to an increase interest for the nanotechnology sector [1, 2] and make their potential use in different areas such as optics, ceramics, electronics and magnetic data storage. For example, one of the specific properties of nanomaterials is that a high percentage of the atoms of the nanoparticle is of the surface. This, highly chemical activity is expected, because the surface atoms are unsaturated so can bind with other atoms very easily [3]. Other important surface related property is the adsorption capacity, because nanomaterials can strongly adsorb many substances including trace metals and polar organic compounds [1] thes providing opportunities to treat contaminants in water [4]. The synthesis of many nanoadsorbents development of new water treatments procedures [5].

As illustrated above, nanomaterials show properties obtendent on surface effects. Other effects are due to influence of size on the intrinsic properties of the materials [6]. Example is magnetic properties of thenanomaterials. Nanoparticles can be classified depending on different parameters, such as their origin (natural or anthropogenic),

formation (biogenic, geogenic, anthropogenic and atmospheric), chemical composition (organic and inorganic), their size, characteristics and shape or applications in research and industry. Examples of different nanostructures are shown in figure 2.

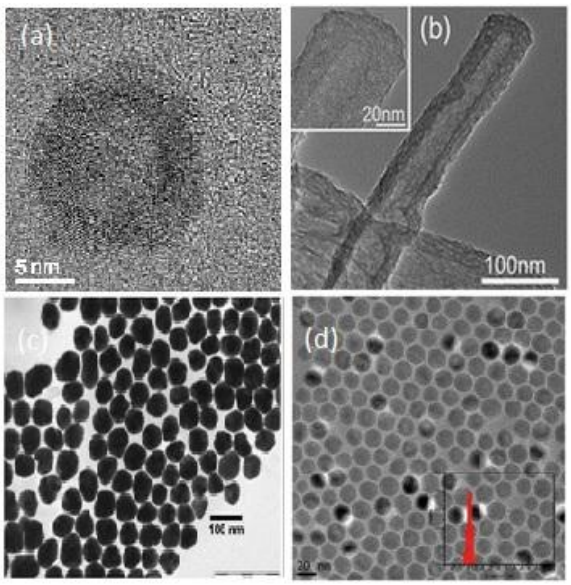

Figure 2. TEM images of (a) quantum dots; (b) mesoporous carbon nanotube; (c) AuNPs; (d) Fe_3O_4 (16,0 ± 1,4 nm) (figure removed from [1,2]

A brief describe of important classes of nanoparticles follows.

1) Carbon-based nanostructures are made up of pure carbon. Carbon-based nanostructures are divided into units groups. Fullerenes, carbon nanotubes (CNTs) and graphene [2]. The simplest form of fullerene is C_{60}, a ball made up from 60 carbon atoms [7] CNTs have different properties and can be synthesized by different methods. These nanotubes have good electrical, mechanical, chemical properties [2] and sorbent properties [1]. Due to their high adsorption capacities, CNTs can be used in many applications such as elimination of pathogens, cyanobacterial toxins and natural organic matter from water systems [2].

2) Metal oxide nanoparticles includes single faced metallic oxide nanoparticles (aluminium trioxide or titanium dioxide), nanostructured mixed oxides (nanostructured binary iron- titanium mixed oxide particles) and also magnetic nanoparticles such as iron

oxides [1]. Metal oxide nanoparticles are employed in different kind of consumer products, for example sunscreens, cosmetics, as catalysts and in biomedicine.

3) Quantum dots. There are fluorescent semiconductor nanocrystals that have been employed for biomedical imaging. Quantum dots have unique optical properties, which depend on their size. When the size is reduced, the surface area to volume ratio increases and surface structure strongly affects on optical and electronic properties [8]. Another important properties of quantum dots are high quantum yield, special chemical properties and high photo- stability. The binary metal dichalcogenides such as CdSe, CdS and ZnS are the most common constituents of quantum dots.

4) Elemental metallic nanoparticles involves inorganic nanoparticles composed, for example of Au or Ag elements but also others metals, like Fe or Zn. Gold nanoparticles are colloids with dimensions ranging from 0,8 – 250 nm and they can be conjugated with different biomolecules through their functional groups and used as elemental markers and chemical anchors [3, 2]. Silver nanoparticles has been employed in consumer products and paints and also as an antimicrobial agent in textiles [9] due to the close contact between the Ag nucleus and the cell walls causing their disruption [2].

5) Magnetic nanoparticles have magnetic properties determined by many factors. One of them are the chemical composition, the type and the degree of defectiveness of the crystal lattice, the particle shape and size, the morphology, the interaction of the particle with the surrounding matrix and the neighboring particles. Changing the nanoparticle size, composition, shape and structure, one can control to an extent the magnetic characteristics of the material based on them. The properties of nanomaterials of the same chemical composition can be different, due to size and surface effects [10].

1.1 Magnetic nanoparticles: fundamental aspects on synthesis and properties

When crystals such as bulk iron are formed from atoms having a net magnetic moment a number of the individual atoms are aligned with respect to each other. In case when the magnetic moments are arranged in the same direction, even when no magnetic field is applied, these materials are called ferromagnetic. These crystals have a magnetic moment and behaves like a bar magnet producing a magnetic field outside of it. While,

ferrimagnetic is made of two types of atoms, each having a magnetic moment of a different strength [11].

Also different types of magnetic materials can be classified according to their magnetic susceptibility. In the first group are materials, which have susceptibility small and negative. These materials are called diamagnetic and their magnetic response opposes the applied external magnetic field. Examples belonging to this group are copper, silver, gold and beryllium. A second group are materials called paramagnets for which susceptibility is small and positive. The magnetization is weak but aligned parallel with the direction of the magnetic field. Examples can be aluminium, platinium and manganese. In many paramagnets the susceptibility is inversely proportional to temperature but in other is independent of temperature. Exist two theories explaining these two types of paramagnetism. First, the localized moment model which leads to the Curie law. Whereas second, the conduction band electron model due to Pauli which leads to temperature-independent and rather weaker susceptibility [12]. Figure 3 illustrates possible arrangements that can occur in two dimensions for magnetic materials.

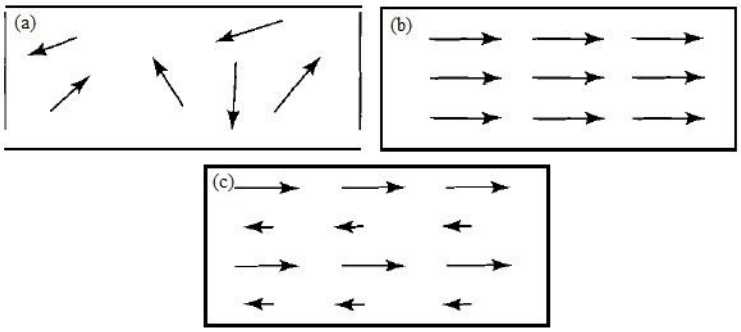

Figure 3. Various arrangements of individual atomic magnetic moments (a) paramagnetic, (b) ferromagnetic, (c) ferrimagnetic [12].

Superparamagnetism is a result of magnetic anisotropy. This is due to the existence of preferred crystallographic directions along which the electron spins are most readily aligned and the substance most easily magnetized. The preferred direction for easy magnetization is along the [111] directions for magnetite. If sufficient energy is supplied, magnetism can be reversed along these axes. Superparamagnetic relaxation occurs when the thermal energy of the particles exceeds the activation energy barrier between the spin

states. The effect of these spin causes that the observed magnetic field is reduced or even absent. Superparamagnetic effect depends on the particle size and on the anisotropy constant. For this reason, this effect is displayed at room temperature by iron oxide nanoparticles less than 10 nm size [13]. Figure 4 shows Weiss domains – phenomena, which is formed due to capabilities of magnetic fields and spins to couple together in very sophisticated ways, generating spin waves and other sorts of weird phenomena. It is visible that superparamagnetism depends on the particle size. Iron oxide crystals are formed by a multitude of Weiss domains within which the magnetic dipoles are parallel to each other. Point 1 on the figure shows nonmagnetic particle, because each Weiss domain has a dipole which is randomly oriented with respect to others. Increase of the applied field causes increasingly alignment of each Weiss domain, till saturation (point 2). Upon a decrease of the applied field to zero, the Weiss domain will be unable to revert to a completely random orientation leading to a remanent magnetization (point 3). Apply a magnetic field of opposite direction and intensity H_C causes cancel magnetization as is shown in point 4 on the graph. This behavior is strongly affected by the size of the particles. Thus, if the crystal is smaller than typical size of a Weiss domain, the magnetic dipole of the particles will return to a zero-average magnetization upon turning off the applied field [14].

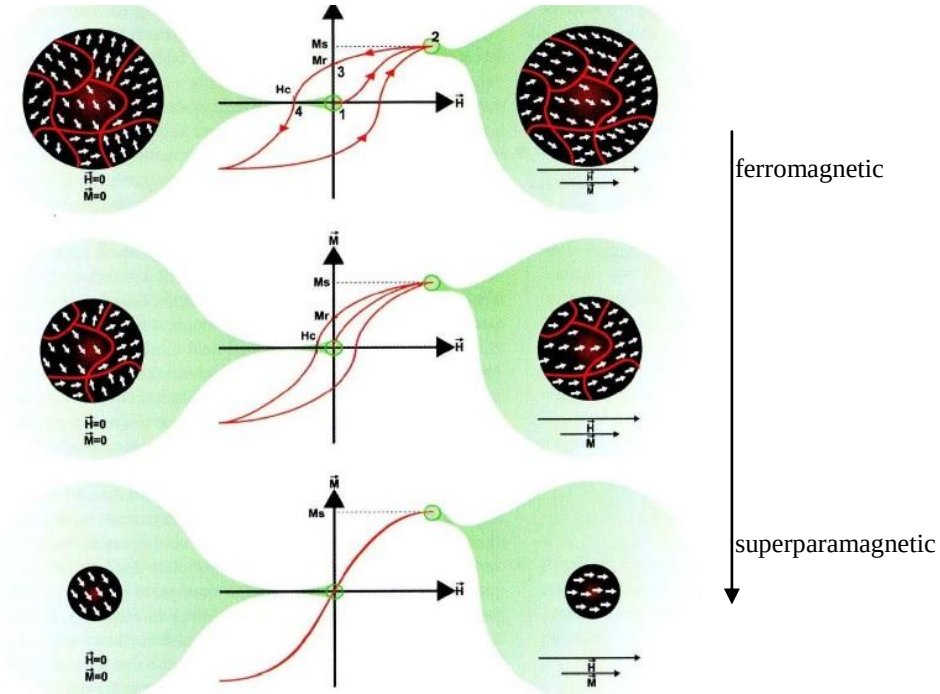

Figure 4. Dependence of magnetic behavior on the particle size [14]

Magnetic nanoparticles are used in a wide range of disciplines like, magnetic fluids, catalysis, biotechnology, biomedicine, magnetic resonance imaging, data storage. Among the magnetic nanoparticles, iron oxides are widely used in chemistry, materials science and physics. Among the several types of iron oxides that have been invesigated in the field of nanosized magnetic particles, maghemite- γ-Fe_2O_3 or magnetite- Fe_3O_4 are the most significant [15] both have superparamagnetic properties at very small sizes. These superparamagnetic nanoparticles have large magnetic moments that make them behave as a giant paramagnetic atoms with a fast response to the external magnetic field and with insignificant remanence and coercivity. Magnetic nanoparticles can be easily attracted to a magnetic field, but after their removal no magnetic property remains thus this characteristic and the resulting low risk of agglomeration, these nanoparticles useful biomedical applications [1] and environmental applications [16]. Magnetic iron oxide is often used because of its low toxicity and price. In addition, iron oxide nanoparticles have high surface to volume ratios, which depend on the particle size. The high surface to volume ratio associated to their ability for surface chemical modification can show enhanced capacity for metal uptake in water treatment procedures [17].

Magnetic nanoparticles have strong magnetic dipole-dipole and Van der Waals attraction. Due to these properties, magnetic nanoparticles tend to aggregate, which can change their magnetic properties, and consequently researchers had the necessity to overcome these aggregation phenomena. This can be done by using desired functional polymers or surfacants coated in the nanoparticles' surface. Surface modification also stabilizes the nanoparticles and precludes their oxidation. The modifying strategies are divided into two groups: (1) coating with inorganic components such as silica and (2) use organic molecules for example octadecylsilane (**ODS**), polymer or surfactant. Silica gel is useful, because is stable under acidic conditions, has high mass exchange, does not swell and shows high thermal resistance. Silica-functionalized magnetic materials are stable under aqueous conditions, and it is easy to control the interparticle interactions and surface modification [13].

Magnetic nanoparticles, such as iron oxides have been synthesized with a number of different compositions and phases. There are many methods for the synthesis of shape-controlled, highly stable and monodispersed magnetic nanoparticles, but techniques like co-precipitation, thermal decomposition, reduction, micelle synthesis, hydrothermal

synthesis and laser pyrolysis can all be directed at the synthesis of high-quality magnetic nanoparticles [18]. Important examples of methods of synthesis for magnetite nanoparticles are describe below.

A facile and convenient method to synthesize magnetite is co-precipitation of Fe(II) and Fe(III) ions, which was described by Massart more than 30 years ago [19]. The reaction takes place according to equation:

$$Fe^{2+} + 2Fe^{3+}8OH^{-} \rightarrow Fe_3O_4 + 4H_2O \qquad (1)$$

The reaction is not direct and other iron species are formed as intermediated:

$$\left(Fe^{3+}\left(H_2O\right)_6\right)^{3+} \rightarrow FeOOH + 3H^{+} + 4H_2O \qquad (2)$$

$$Fe^{2+} + 2OH^{-} \rightarrow Fe\left(OH\right)_2 \qquad (3)$$

$$2FeOOH + Fe\left(OH\right)_2 \rightarrow Fe_3O_4 + 2H_2O \qquad (4)$$

This method consist of synthesis of iron oxide from aqueous Fe^{2+}/Fe^{3+} salt solutions by the addition of a base under inert atmosphere at room temperature or at slightly temperature. Factors such as the type of salts used (usually chlorides, sulfates and nitrates), the Fe^{2+}/Fe^{3+} ratio, the pH value, ionic strength of the media and the reaction temperature affect on the size, shape and composition of the magnetic nanoparticles [18]. The temperature, the effect of heating the precipitate in the alkaline medium and the effect of addition of surfactant to the reaction mixture affect on particle size. When uncoated particles are heated in the alkaline medium then particle size increases [20].

Another method is thermal decomposition, which is inspired by the synthesis of high-quality semiconductor nanocrystals and oxides in non-aqueous media. This method of metal-containing compounds has been studied in detail in relation to the development of the scientific grounds of the metal organic chemical vapour depisition technique. Through this method one can obtain high quality nanoparticles [21]. Similar methods for the synthesis of magnetic particles, with control over size and shape have been developed [18]. For example Yang et al. [22] synthesized iron oxide nanorods by thermal decomposition of $[Fe(CO)_5]$ in ionic liquid [23]. Also Butter et al. [24] used this compound in the presence of polyisobutene in decalin under nitrogen atmosphere at 170ºC.

A method which includes amphoteric surfactants to create water-swollen reversed micellar structures in nonpolar solvents, is reverse micelles and micro-emulsion technology [25]. This method is a thermodynamically stable isotropic dispersion of two immiscible liquids. Between which is microdomain, which is stabilized by an interfacial film of surfactant molecules [26]. Microemulsions can be prepared by addition of for example pentanol, hexanol or butanol to milky emulsions to make transparent solutions comprising dispersions of either water-in-oil or oil-in-water in nanometer or colloidal dispersions [27]. In water-in-oil microemulsions, the aqueous phase forms microdroplets, which size is typically 1-50 nm in diameter, surrounded by a monolayer of surfactant molecules in the continuous hydrocarbon phase [18]. When the soluble metal salt is incorporated in the aqueous phase of the microemulsion, it will reside in the aqueous microdroplets surrounded by oil. These microdroplets will continuously collide, coalesce and break again [28]. Addition of solvents, such as acetone or ethanol, to the microemulsions can facilitate the extract of precipitate by filtering or centrifuging the mixture. In this sense, a microemulsion can be used as a nanoreactor for the formation of nanoparticles [18]. The main advantage of the reverse micelle or emulsion technology is the diversity of nanoparticles that can be formed by varying the nature and amount of surfactant and cosurfacant, the oil phase, or the reacting conditions. In addition, by changing temperature and the surfactant concentration, the size of the magnetite can be controlled [25]. This method has many advantages, but also has disadvantages. One of them is low yield of nanoparticles compared to other methods, such as thermal decomposition and co-precipitation. Large amounts of solvent are necessary to synthesize significant amounts of material. Though many advantages, this method is not very efficient process and also rather difficult to scale-up [18].

Under hydrothermal conditions a broad range of nanostructured materials can be formed [18]. Hydrothermal synthesis is performed in aqueous media in reactors or autoclaves where the pressure is higher than 2000 psi and the temperature can be above 200ºC [25]. There are two ways for the formation of magnetite via hydrothermal conditions. First is hydrolysis and oxidation; second- neutralization of mixed metal hydroxides. Both are very similar, except that only ferrous slats are used in the first method. The reaction conditions, such as solvent, time and temperature have very important effects on the products. It was observed that particle size of Fe_3O_4 powders

increased with long reaction time and that higher water content resulted in the precipitation of larger magnetite particles [29]. During hydrothermal process, the particle size is controlled through the rate processes of nucleation and grain growth [25].

Table 1 shows advantages and disadvantages of the four above-mentioned methods. Considering the simplicity of the synthesis, co-precipitation is the preferred route. In terms of morphology and size control of the nanoparticles, thermal decomposition seems the best method developed to date. Also microemulsions can be used to synthesize monodispersed nanoparticles with various morphologies, but this method has disadvantages, mainly that requires a large amount of solvent. High-quality nanoparticles can be synthesized by hydrothermal synthesis but is a relatively little explored method. To sum up, co-precipitation and thermal decomposition are the best studied methods which allow prepared nanoparticles on a large scale.

Table 1. Comparise of the synthetic methods for magnetite nanoparticles [18]

Method	**Synthesis**	**Reaction temp. [ºC]**	**Solvent**	**Size distribution**	**Shape control**	**Yield**
Co-precipitation	Very simple, ambient conditions	20-90	Water	Relatively narrow	Not good	High/scalable
Thermal decomposition	inert atmosphere	100-320	Organic compound	Very narrow	Very good	High/scalable
Microemulsion	ambient conditions	20-50	Organic compound	Relatively narrow	Good	Low
Hydrothermal synthesis	Simple, high pressure	220	Water-ethanol	Very narrow	Very good	Medium

Chemical composition, size, shape and structure play a major role in the particular and special properties that characterize nanoparticles and their environmental and health impact [2]. Transmission Electron Microscopy (**TEM**), Scanning Electron Microscopy (**SEM**), Fourier Transform Infrared spectroscopy (**FTIR**), Powder X-ray Diffraction (**XRD**) Technique, Thermogravimetric Analysis (**TGA**) are methods widely used in the literature for Fe_3O_4 nanoparticle characterization and surface determination [25].

There are several investigated methods to determine the sizes characterizing nanoparticles. "Size" can be define in two different ways. First, include different parts of the nanoparticles, such as the whole iron core, the crystalline part of the core, the core, the shell and the hydrated layer. In this case, size can also be interpreted as a no geometrical meaning on the particle but just a physical meaning. Second, nanoparticles are polydisperse. This double meaning of size gives rise to different values depending if the technique gives access to a volume, intensity or number [29].

Among the methods used for the determination of the size and size distribution of nanoparticles is TEM [27] and DLS [25]. This technique is used for measuring the size of particles typically in the submicron region. In dynamic light scattering, the speed at which the particles are diffusing due to Brownian motion is measured. This is possible by measuring the rate at which the intensity of the scattered light fluctuates when detected using a suitable optical arrangement. Concentration of particle suspension, composition of solvents, dust and other additivies, such as ions or free radicals may affect on the particle size distribution measurement [30]. DLS has many advantages for sizing magnetic nanoparticles, first of all, the measuring time for DLS is short and it is almost all automated. This technique does not destroy the sample, so its can be employed for other purposes after the measurement and is extremely sensitive towards the presence of small aggregates [31]. Only one disadvantage is impossibility use to analyze as powders or solids, because DLS is limited to dilute colloids [25].

Also TEM have been employed to measure the size or size distribution of magnetic nanoparticles. This technique can give the total particle size of the core and gives access to a number-weighted mean value [29]. The use of the short wavelengths achievable with highly accelerated electrons is possible to investigate the structure of magnetic nanoparticles down to the atomic level of detail, whereas by performing image analysis on the TEM micrograph obtained, it is possible to give quantitative results on the size

distribution of the magnetic nanoparticles. A typical nanoparticles suspension composed of 10^{10} to 10^{15} particles/mL, give a relatively small sample pool to draw statistically conclusive remarks [31].

The SEM technique provides information about the sample's morphology, surface, elemental composition, shape, size and other properties such as electrical conductivity [2]. The sample preparation is simple, because some nanomaterials can be observed by SEM directly through loading them on carbon tape but size can limit observation [32]. Useful technique to determine the crystal structure and characterization of Fe_3O_4 nanoparticles, is Powder XRD [25]. This technique is highly surface-specific and gives information on coatings and surface properties or elemental composition.

Other techniques, such as thermogravimetric analysis (**TGA**) and FTIR, have been used to examine the surface properties of coated iron oxide nanoparticles [29]. FTIR have been used to characterize the phase of the magnetic core of magnetite nanoparticles [25]. FTIR is useful, because without any specific preparation, allows characterization of molecular or chemical composition of many types of samples [33]. The use of FTIR can be useful to check the chemical achievement between the Fe_3O_4 core and the organic surface coverage [34]. For the determination of the weight of surfactant, which covered the particle surface per mass of magnetite and for the determination of desorption binding heat of the covering layers used thermogravimetric analysis [25].

Table 2. Nanoparticle characterization techniques [2]

Characterization technique		**Information provided**
Microscopic techniques	SEM	Surface, size, shape morphology, crysrallographic composition
	TEM	Elemental composition, electrical conductivity
X-ray based techniques	XRD	Surface, crystallographic and elemental composition
Light scattering	DLS	Particle size

1.2 Bionanocomposites of magnetite

Research on bionanocomposites brings together biology, material science and nanotechnology. The main task in the design and fabrication of all composites has been to combine two or more different materials to produce a single material, which must behave as a homogenous entity and has predictable and reproducible properties. Proper design, composite combines the best qualities of each component and allows to produce a material with some properties [35].

Biopolymer nanocomposites are the result of the combination of biopolymers and inorganic solids at the nanometer scale. They could be formed from different biopolymers, such as polypeptides, proteins, nucleic acids and polysacharides, but also from inorganic solid particles, for example layered silicates, hydroxyapatite, metal oxides and silica [36]. They can act as molecular bridges in the polymer matrix, because enables interaction between the filler components and the matrix. This is the basis for enhanced mechanical, thermal, biological, magnetic, electronic, optical and optoelectronic properties as compared with the corresponding inorganic or polymer components [35]. Possibility of applications are related to their thermal, mechanical and barrier properties, making bionanocomposites useful for uses in controlled drug and pesticides delivery, membranes for food processing, drinking water purification, oxygen barrier films and food package. In addition, bionanocomposites can be used as biomedical materials, because they are biocompatible and biodegradable compounds [36]. In table 3 are presented some advantages and shortcomings of biopolymers.

Table 3. Key advantages and shortcomings of biopolymers [37]

	Advantages	**Shortcomings**
Biopolymers	Limited environmental impact, low cost	Low mechanical strength
	Favorable interactions with living systems	High degradation rate
	Chemical and structural diversity	Preformed polymers
	Hierarchically organized structures	-
	Dynamic properties	
	Molecular recognition and bioresponsiveness	

Silica is a material, which can be used to coat magnetic nanoparticles. These coatings prevents their aggregation in liquid, improves their chemical stability, provides better protection against toxicity and can also help in binding various biological ligands to the nanoparticle surface. There are different ways to generate magnetic silica nanospheres. One of them is the well-known Stöber process, in which silica was formed *in situ* through the hydrolysis and condensation of a sol-gel precursor, such as tetraethyl orthosilicate (**TEOS**). The surfaces of silica-coated magnetic nanoparticles are hydrophilic and are easily modified with other functional groups [18]. This method was successfully used by Im et al. [38], which showed that the final size of silica the coated colloids depends upon the concentration of iron oxide nanoparticles and the type of solvent. This is due to the fact that the size of the coated silica particles is closely related to the number of iron oxide seeds. Larger particles were obtained at lower concentrations of iron oxide nanoparticles and in alcohols with higher molecular weights [29]. The attachment of silane-coupling materials, such as, to a nano-object is made using one or several covalent bonds to link the matrix to a precursor [1, 29]. These materials are able to form covalent bonds with bioaffinity adsorbents through organofunctionalities [29]. A scheme of the silane-coupling process is shown in figure 5, for cubic magnetite particles coated with SiO_2.

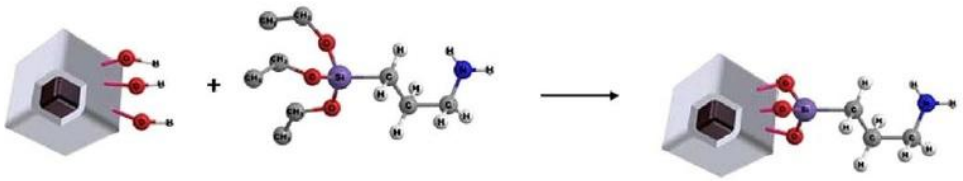

Figure 5. Chemical functionalization of the silica shells at the magnetite surfaces [11]

Silica nanoporous materials have been often used due to their properties, such as high surface area. Modified silica can be used for preconcentration of organic pollutants and many metal ions [1]. Another advantage is the presence of surface silanol groups that can easily react with various coupling agents to attach specific ligands to magnetic particles. A good example can be amine groups, which have been introduced on the surface of silica-coated magnetite nanoparticles by condensation and hydrolysis of an organosilane, such as 3-aminopropyltriethoxysilane (**APTES**), on the surface of magnetite nanoparticles [29].

A methods for the introduction of amine groups onto the surface of magnetite and silica coated magnetite nanoparticles have been reported. Amine modified particles can be used to covalently link specific biomolecules [39], drugs and other organic compounds [40], generaly "bioactive" nanoparticles [37]. Figure 6 presents a scheme of the surface modification of nanoparticles by APTS. In solution phase, the hydrolysis of the alkoxysilane molecules results into highly reactive silanol species while on the solid phase their condensation with surface free –OH groups render strong Si-O-Si bonds, forming a SiO_2 shell at the surface of the particles [39].

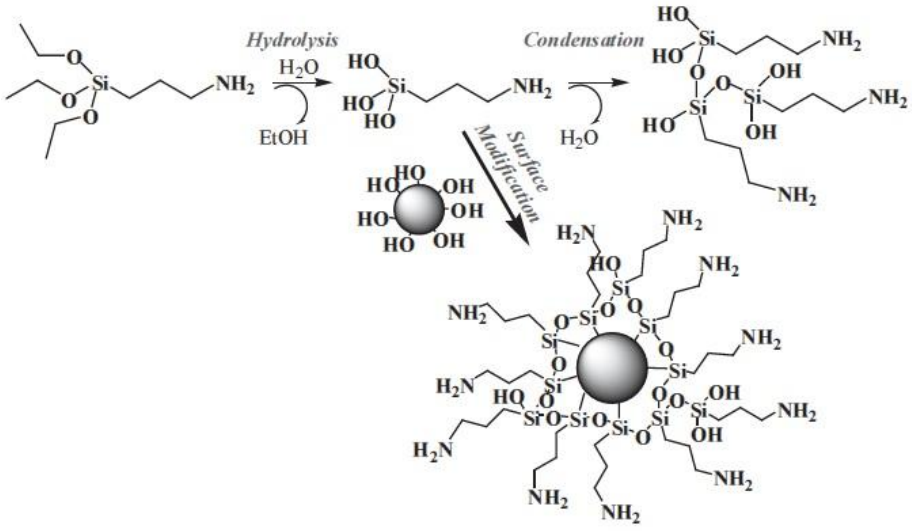

Figure 6. Surface modification of SiO_2 nanoparticles using APTES [39]

1.3 Sorbents for metal complexes in water

Among the several applications of bionanocomposites has been also investigated water purification. Contamination of water with toxic metal ions such as Cr^{3+}, Ni^{2+}, Co^{2+}, Hg^{2+} or Pb^{2+} is a severe environmental and public health problem. Various techniques such as adsorption, precipitation, ion exchange, reverse osmosis, electrochemical treatment, membrane filtration, evaporation, flotation, oxidation and biosorption have been extensively used. Among these, adsorption is an selective technique to remove toxic metal ions from water. For water purification numerous adsorbents have been developed, but magnetic nanoparticles functionalized with biocompatible organic/inorganic molecules are

more effective, because of the surface there are functional groups, which provide a large number of active sites, for the successful adsorption of metal ions [40].

A schematic representation of a possible mechanism for the adsorption of metal ions by amine functionalized magnetic nanoparticles is shown in figure 7. In this representation, the effect of pH has been highlighted.

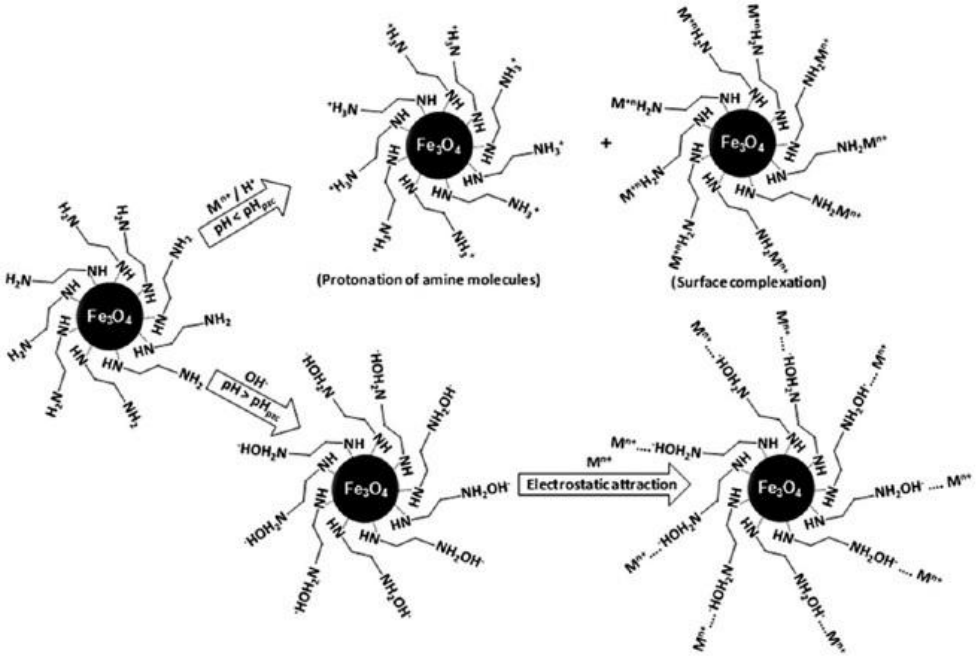

Figure 7. A possible mechanism for adsorption of metal ions by amine functionalized magnetic nanoparticles [40]

At pH< pH_{pzc} (pH of zero point charge) the protonation of amine groups ($-NH_3^+$) and surface complexation of metal ions ($-NH_2M^{n+}$) may occur of on the surface of amine magnetic nanoparticles. Conversion of $-NH_2$ groups to $-NH_3^+$ causes fewer $-NH_2$ sites available of the Fe_3O_4 surfaces for the adsorption of metal ions through complexation. The large number of $-NH_3^+$ causes increase of the electrostatic repulsion between M^{n+} and surfaces of magnetite. All these effects can affect on the reduction of M^{n+} adsorption on amine magnetic nanoparticles at low pH. At higher pH the surface of amine magnetic nanoparticles is negatively charged due to the formation of $-NH_2OH^-$. Thus, the adsorption

of metal ions increases with increasing pH of the solution, which can give almost 100% removal for certain metal ions [41].

Heavy metal pollution is a serious environmental and public health problem in many places worldwide. Chromium is one of the most toxic metal endangering human life. Cr(III) ion compounds are used in leather making, wood preservation, textile dyeing, metal finishing and petroleum refining. The wide use of chromium ions increases the risks of water pollution. This is extremely harmful to human beings because Cr(III) ions can change the valence from III to VI causes formation of Cr(VI) ions. There are non-biodegradable in living tissues and would induce toxic and carcinogenic health effects on humans [42]. Therefore, it has become increasingly urgent to develop new technologies for heavy metals removal from industrial effluents. As mentioned previously, for this purpose several methods have been used such as, adsorption and biosorption processes. Among these techniques, some of these, can be very expensive and sometimes not very effective [43]. All these facts resulted in an increased interest to explore other adsorbents to replace expensive materials, particularly low-cost raw materials such as agricultural by-products, residual polymer materials, carbonized coals or wood materials.

One material that has been studied as adsorbent is rice husk. This material is a renewable agricultural residue and is a by-product from the rice milling industry. Rice husks have granular structure, chemical stability, mechanical strength and water insolubility. This type of adsorbent has already been successfully applied for the removal of lead [44], mercury [45], gold [46] and chromium [47]. Other low-cost materials for metal removal from water include wastes from industrial processes such as cork and yohimbe bark, grape stalks and olive pits [48]. Other examples of biosorbents are sawdust [49], oil palm [45] and tea leaves [51].

Other type of adsorbents that may be very useful for removing inorganic contaminants from water, are modified biopolymers and hydrogels. This is due to their particular structure, pshychico-chemical characteristics, chemical stability, high reactivity and selectivity towards heavy metal ions, resulting from the presence of reactive chemical groups in polymer chains. Among the group of biopolymers, polysaccharides appear as renewable and biodegradable resources, having a capacity to associate with a wide variety of molecules by physical and chemical interactions. As important and useful polysaccharide is alginate (figure 8), which has the ability to complex various heavy metal

ions [52]. Alginic acid is a linear, binary copolymer of 1,4-linked α-L-guluronic acid and β-D-mannuronic acid, which is isolated from brown algae but is also present in some species of bacteria [53]. Alginate has a lot advantages such as, biodegradability, hydrophilicity and stability in wide pH range [54]. In addition, is a good sorbent of metal ions because has the ability to form gels by ion-exchange reaction with multivalent metal ions [53]. Has been studied that efficiency of absorption of Cr(III) might be high as 0,14 g per gram of dry alginate beads [40].

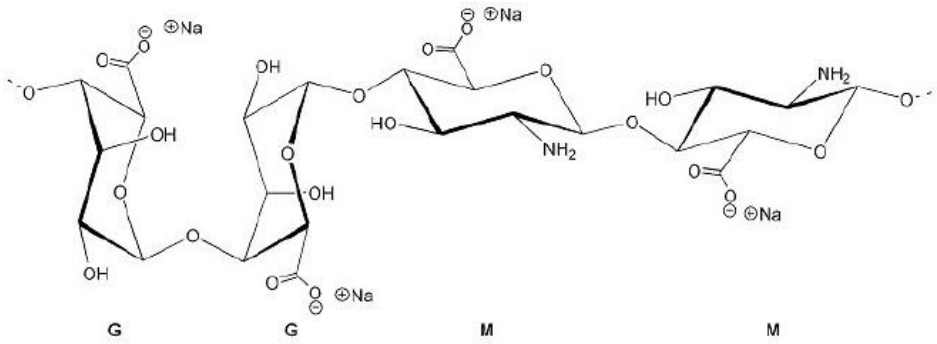

Figure 8. Structure of sodium alginate polymer [54]

In view of the many applications of alginate and iron oxide, several strategies for the preparation of iron oxide nanoparticles with alginate have been developed. The standard chemical synthesis consist of three steps including gelation of alginate and ferrous ion; in situ precipitation of ferrous hydroxide by the alkaline treatment of alginate; and oxidation of ferrous hydroxide with an oxidizing agent [56]. Second method, develop by Ma et al. [56], involves two-step coprecipitation method- (a) formation of Fe_3O_4 particles by coprecipitation of ferric and ferrous ion with alkaline solution, (b) combination of Fe_3O_4 particles to alginate. This method is easier and the obtained iron oxide nanoparticles coated with alginate show good colloid stability. The reason for these stability is because alginate provides many surface carboxylic groups. These groups interact with iron ions as well as originate electrostatic repulsions between the coated iron oxide nanoparticles [56].

Chitin and chitosan (figure 9) are two natural materials that have also been used to remove metal ions from water. The first one is extracted from crustacean shells, which are waste products of seafood processing industries. Chitin is the second most abundant

polymer in nature after cellulose, whereas, chitosan can be formed by deacetylation of chitin. The chitosan has drawn particular attention for its feasible application in a variety of forms, from flake-types to gels, beads and fibers [57]. Because of the high content of aminic and hydroxyl groups in chitosan, this by-product material has been found to be able to adsorb several metal ions including those of chromium [58] and lead [57]. According to Keng et al. [57], the extension of metal adsorption by this material depends strongly on the chitosan source, deacetylation degree, nature of metal ion, variations in crystallinity, amino content and solution pH.

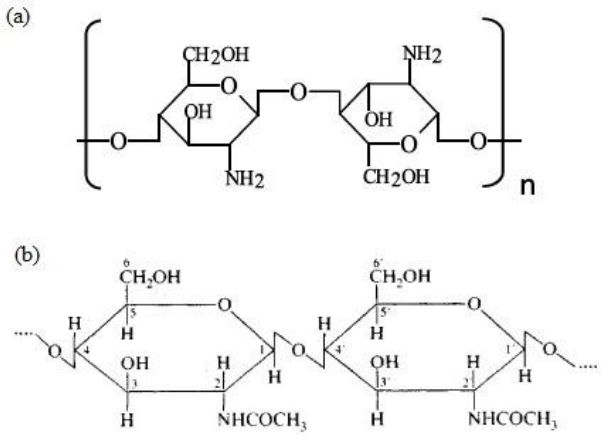

Figure 9. Molecular structure of (a) chitosan [58] and (b) chitin

Yantasee et al. [59] prepared iron oxide nanoparticles, which were functionalized with dimercaptosuccinic acid (**DMSA**). This way allowed to prepare a novel dispersible sorbent, which can be magnetically collected and has a high capacity and selectivity for the softer heavy metals. Hg(II), Ag(I), Pb(II), Cd(II) and Tl(I) ions effectively bind to the DMSA ligands, while As(III) binds to the iron oxide lattices. In the article is described also the ease with which nanoparticles can be separated from solution- within a minute using a magnet. The authors compared the chemical affinity, capacity, kinetics and stability of the magnetic nanoparticles to those of conventional resin based sorbents, activated carbon and nanoporous silica of similar surface chemistries in river water, ground water and seawater. These studies have shown an advantage of iron oxide functionalized with DMSA.

DMSAFe_3O_4 showed a capacity of 227 mg of Hg/g, a 30-fold larger value than that of resin based sorbents.

Liu et al. [55] have studied a novel low-cost magnetic sorbent material prepared by coating Fe_3O_4 magnetic nanoparticles with humic acid (**HA**). These nanoparticles were developed for the removal of heavy metal ions, such as Hg(II), Pb(II), Cd(II) and Cu(II) from water. HA has high affinity to magnetite and in the use its functionalization have a number of advantages. One of them is that sorption of HA on the Fe_3O_4 nanoparticles enhanced the stability of nanodispersions by preventing their aggregation. This acid has a skeleton of alkyl and aromatic units that comprises carboxylic acid, phenolic hydroxyl and quinone functional groups. Due to these functional groups, which have high coordination capacity for heavy metal ions, HA was applied to remove heavy metal ions from water. These studies have shown that sorption of the heavy metals to Fe_3O_4/HA reached equilibrium in less than 15 min and agreed to the Langmuir adsorption model with maximum adsorption capacites ranging from 45 to 100 mg/g. 99% of Hg(II) and Pb(II), and over 95% of Cu(II) and Cd(II) were removed from tap water at optimized pH.

Also amino groups were used to functionalization of magnetic nanoparticles. Wang et al. [61] developed amino-functionalized magnetic nanomaterial by covalently grafting amino groups onto the surfaces of Fe_3O_4@SiO_2. This material was used to remove heavy metal ions from aqueous media. Cu(II), Co(II), Ni(II), Zn(II), Pb(II) and Cd(II) ions can be removed from aqueous solution owing to the strong metal complexing capability of amino groups. In fact, amino-functionalized nanoadsorbent exhibited high affinity for aqueous Cu(II), Pb(II) and Cd(II) ions. In this study the results of adsorption affinity were not much satisfactory. The reason for this was the presence of a cosolute of HA or alkali/earth metal ions (Na^+, K^+, etc.). Fe_3O_4@SiO_2-NH_2 nanoparticles were easily recovered from aqueous solution by magnetic separation and regenerated easily by acid treatment.

Singh et al. [41] have used Fe_3O_4 magnetic nanoparticles functionalized with amine groups for removal of Cr^{3+} ions from water. Experiment showed that removal efficiency of metal ions is strongly dependent on pH of the solution, which is seen in figure 10. The removal of ions increase with increasing pH of the solution till extraction rates approach a plateau. About pH 6 obtained almost 100% removal of Cr^{3+} ions from waste-water. The experiment carried out with different concentration of nanoadsorbents. This confirmed that the removal efficiency of metal ions is also dependent on the concentration of

nanoadsorbents- adsorption of metal ions increases with increasing the concentration of nanoadsorbents.

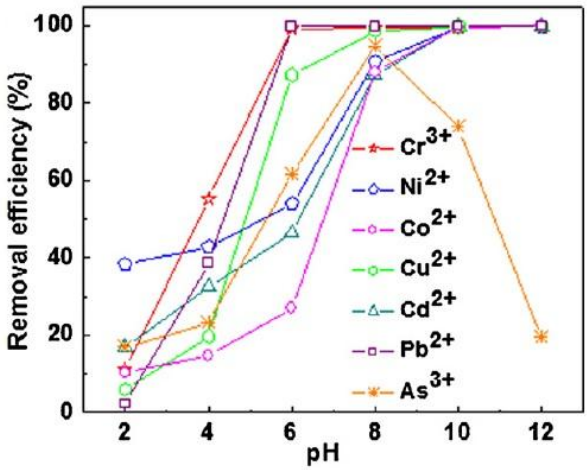

Figure 10. pH dependent removal efficiency of some metal ions by amine functionalized nanoparticles [41]

Salicylic acid (**SA**) is a commercial ligand with a carboxylic and a phenolic function site which can act as electron donor reacting with most of hard and intermediate cations. For these reasons Shishehbore et al. [62] developed a method for the pre-concentration of trace heavy metal ions in environmental samples. It consist in the sorption of Cu(II), Cd(II), Ni(II) and Cr(III) ions with SA as chelate on silica-coated magnetite nanoparticles. Figure 11 shows steps of synthesis of magnetic nanoparticles with SA and also solid phase extraction of the analytes.

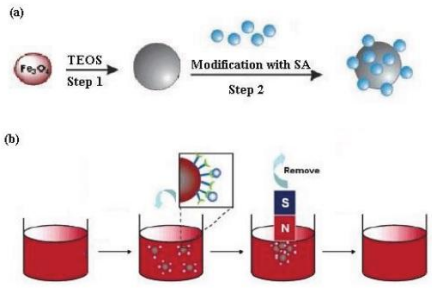

Figure 11. Schematic of the preparation of adsorbent (a) and solid phase extraction of the analytes (b) [62]

The solution pH is an important parameter to obtain quantitative recovery for heavy metal ions which may confirm figure 12. Could be seen that quantitative recovery was obtained for metal ions within the pH range 5-7 and the decrease in recovery at pH values lower than 5. May be this due to the competition of proton with cations in binding to donor atoms. In fact, the method was successfully applied to the evaluation of these trace and toxic metals in various waters.

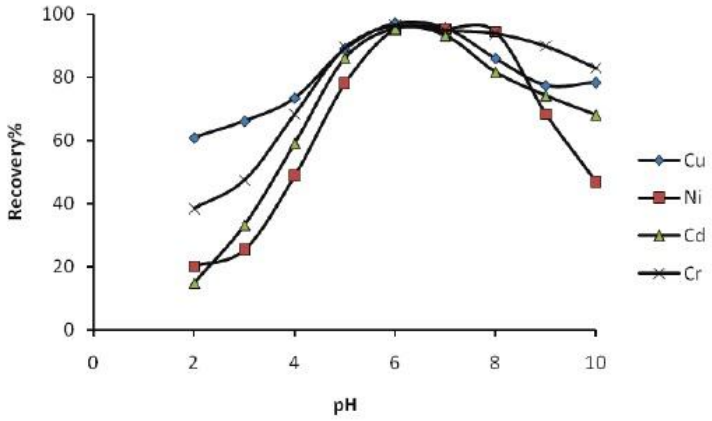

Figure 12. Recovery of metal ions in function of pH, using salicylic acid [62]

All the methods described above are summarized in table 4.

Table 4. Examples of surface modified magnetite nanoparticles for the removal of heavy metal ions from water

Synthesis method	Coating agents	Surface functionalized group	Metal removed	Ref
Thermolysis of precursors	Dimercaptosuccinic acid	Thiol group	Hg(II), Ag(I), Pb(II), Cd(II)	[59]
Co-precipitation	Humic acid	Carboxylic and phenolic group	Hg(II), Pb(II), Cd(II), Cu(II)	[60]
Co-precipitation followed by a sol-gel process using sodium silicate	(3-aminopropyl)trimethoxysilane	Amine group	Pb(II), Cd(II), Cu(II)	[61]
Thermolysis of precursors	ethylenediamine	Amine group	Cr(III), Co(II), Ni(II), Cu(II), Cd(II), Pb(II), As(III)	[41]
Co-precipitation followed by hydrolysis of TEOS	Salicylic acid Functionalized silica	Carboxylic group	Cr(III), Cu(II), Cd(II), Ni(II)	[62]

1.4 Objectives and outline

Over the past decade, there has been great interest for nanoparticles as new sorbents due to their unique size/surface dependent properties and possibility for removal of several pollutants from wastewaters using adequate surface chemical functionalization.

In spite of the many advantages, colloidal nanoparticles might have also limitations related to their colloidal instability over long periods of time. Small particles tend to form agglomerates in order to reduce the energy associated with the high surface area per volume ratio. Therefore it is necessary to develop coating strategies to chemically improve the stability of colloidal magnetic nanoparticles because this is a crucial requirement for their application as nanosorbents. Concerning magnetite nanoparticles, there are no reports on the use of alginate as a coating material aiming sorption applications. Therefore the main objective of this thesis was to investigate the use of this polysaccharide as a coating material over magnetite nanoparticles aiming sorption applications. In particular, the covalent attachment of alginate to silica modified magnetite surfaces was investigated and the final materials were evaluated as sorbents for Cr(III) species dissolved in water.

Hence, in a first part of the thesis, magnetite nanoparticles coated with silica shells have been functionalized with a coupling agent containing amine groups and then these materials have been functionalized with alginate. These materials have been characterized using several techniques such as FTIR spectroscopy, powder X-ray diffraction, thermogravimetric analysis, zeta potential measurements, elemental analysis and TEM. In a second stage, the magnetic nanoparticles functionalized with alginate were evaluated as magnetic sorbents for the removal of [Cr(HY)(H_2O)] complex and Cr(III) ions dissolved in water.

The time profile for the adsorption behavior of those species onto magnetic nanoparticles was assessed in order to investigate the kinetics involved. This model describes the uptake rate of adsorbate, which in turn controls the resident time in the adsorbent-solution interface. Several theoretical models have been used in order to explain the sorption kinetics of the new materials in various experimental conditions. The results of this research show that the covalent attachment of alginate to the magnetic nanoparticles was successful and these new hybrid materials have potential as colloidal nanosorbents.

2. Experimental

2.1 Chemicals

Ferrous sulfate heptahydrated ($FeSO_4 \cdot 7H_2O$) (>99%) and ethanol (C_2H_5OH) (>99%) were obtained from Panreac (Spain). Potassium nitrate (KNO_3) (>99%), tetraethyl ortosilicate ($Si(OC_2H_5)_4$; TEOS, >99%) and 3-aminopropyltrimethoxysilane ($H_2N(CH_2)_3Si(OCH_3)_3$, APTMS, >99%), N-hydroxysuccinimide ($C_4H_5NO_3$, NHS, >98%), disodium salt of ethylenediaminetetraacetic acid ($[-CH_2N(CH_2CO_2Na)CH_2CO_2H]_2$, EDTA-$Na_2$ >99%), N-(3-dimethylaminopropyl)-N'-ethylcarbodiimide hydrochloride ($C_8H_{17}N_3 \cdot HCl$, EDC >99%), alginic acid sodium salt from brown algae and potassium chloride (KCl) (>99%) were purchased from Sigma-Aldrich. Potassium hydroxide (KOH) (>86%) and sodium hydroxide (NaOH) (>98%) were purchased from Pronolab (Portugal). Ammonia (NH_4OH) (25% NH_3) was purchased from Riedel-de-Häen (Germany) and hydrochloric acid (HCl) (37%) from Fluka Chemie (Denmark). All chemicals were used as received.

2.2 Synthesis of magnetite (Fe_3O_4) nanoparticles

Magnetic iron oxide nanoparticles were synthesized by oxidative hydrolysis of iron (II) sulphate in alkaline conditions. 25 mL of deoxygenated water, which was first deoxygenated with N_2 under vigorous stirring during 2 hours, was added to a 250 mL round flask. Then, 1,98g and 1,5327 g of KOH and KNO_3 respectively were added. The mixture was heated at 60ºC with bubbling N_2 and mechanically stirred at 500 rpm. When salt was dissolved, 25 mL of an aqueous solution containing 4,775 g of $FeSO_4 \cdot 7H_2O$ was added drop-by-drop and the stirring was increased to 700 rpm. The resulting solution presented a dark-green color after complete addition of Fe^{2+} salt. After the addition of all above mentioned compounds, the solution was left to react for 30 min at 60ºC. After reaction, the temperature was increased to 90ºC and the mixture was left under N_2 with no stirring during 4 hours.

The resulting black powder was washed several times with deoxygenated water and ethanol and collected using a NdFeB magnet. After washing, the particles were dried by evaporating the solvent at 60ºC.

2.3 Coating of magnetite nanoparticles with an amorphous silica shell functionalized with amine groups (Fe_3O_4@SiO_2-NH_2)

Silica coating of the magnetite and amino-functionalized magnetite@SiO_2 was performed in one unique step in the following way: 50 mg of Fe_3O_4 nanoparticles were added to 80 mL ethanol and then the suspension was left to sonicate for 10 min, allowing for the particles to be highly dispersed in the solution. After, 100 µL of TEOS, 3 mL of ammonia (25%) and 35 µL of APTMS were added to the solution which was left for 2 hours at room temperature under sonification. The resulting particles were washed with distilled water and ethanol. The powder was then collected magnetically from the suspension. After washing, particles were left to dry by solvent evaporation at 60ºC.

2.4 Covalent attachment of alginate to the magnetic particles (Fe_3O_4@SiO_2-NH_2-ALG)

For the covalent attachment of alginate to the magnetite two solutions were prepared. The first one comprised 50 mg of alginate dissolved in 5 mL distilled water to which 20 mg and 25 mg of EDC and NHS, respectively, were added. This is necessary because the reaction between the –NH_2 groups of the surface of the particles and the –COOH groups of the alginate is achieved by carbodiimide activation, using EDC and NHS. The second solution comprised 30 mg of Fe_3O_4@SiO_2-NH_2 nanoparticles dispersed in distilled water (5 mL). Then, the second solution was added to the first solution and the pH was adjusted to 4,5 by adding 865 µL of 0,01 M HCl and 40 µL of 0,1 M HCl. The resulting suspension was stirred for 24 h, at room temperature (23ºC) using a mini rotator. After 24 h the nanoparticles were magnetically recovered using a NdFeB magnet, rinsed with distilled water and freeze-dried.

2.5 Synthesis of [Cr(HY)(H_2O)]

0,93 g of EDTA-Na_2, was added to a solution of 1 g of $Cr(NO_3)_3 \cdot 9H_2O$, previously dissolved in 13 mL of hot water, under vigorous stirring. Then, the resulting purple

solution was heated, with constant stirring, at a temperature slightly lower than boiling temperature for 30 minutes. At the end the formation of a purple solid has been observed. After reaction the mixture was left to cool at room temperature. The formed crystals were filtered and washed with 10 mL of distilled water and then with a little ethanol. After this, the crystals were dried at room temperature.

2.6 Instrumentation

Fourier transform infrared (FTIR) spectra of the Fe_3O_4, Fe_3O_4@SiO_2-NH_2, Fe_3O_4@SiO_2-NH_2-ALG and [Cr(HY)(H_2O)] were collected using a spectrometer Bruker optics tensor 27 coupled to a horizontal attenuated total reflectance (ATR) cell, using 128 scans at a resolution of 2 cm^{-1}. The crystallite phase of the magnetic nanoparticles was identified by powder X-ray diffraction (XRD). The X-ray powder diffraction patterns of the samples were recorded using X-ray diffractometer Philips X'Pert equipped with a Cu Kα monochromatic radiation source. The alginate content in the functionalzed magnetic nanoparticles was calculated by thermogravimetric analysis (TGA). These experiments were performed using a TGA 50 from a Shimadzu instrument. Samples were heated from 25ºC to 900ºC at 10ºC min^{-1}, under nitrogen atmosphere. The surface charge of the Fe_3O_4, Fe_3O_4@SiO_2-NH_2 and Fe_3O_4@SiO_2-NH_2-ALG were assessed by zeta potential measurements, using a Zeta-sizer Nanoseries instrument from Malvern Instruments. The zeta potential measurements were performed in aqueous solutions prepared with distilled water. Elemental analysis (C, H and N) was performed by Truspec 630-200-200 at combustion furnance temperature 1075ºC. Carbon and hydrogen were detected using infrared absorption and nitrogen using thermal conductivity. The morphology and size of bare and coated nanoparticles was investigated by transmission electron microscopy (TEM). For this purpose, used a transmission electron microscope Hitachi 9000 operating at an accelerating voltage of 300 kV. Samples were prepared by evaporating dilute suspensions of the nanoparticles on a copper grid coated with an amorphous carbon film.

2.7 Adsorption experiments

The nanomaterials described above were investigated for the uptake of [Cr(HY)(H_2O)] complex and Cr(III) ions from water, using Fe_3O_4@SiO_2-NH_2 and Fe_3O_4@SiO_2-NH_2-ALG nanoparticles respectively. As a source of Cr(III) used $Cr(NO_3)_3 \cdot 9H_2O$. Experimental solutions of the desired concentrations were obtained by succesive dilution. The pH of the solution was adjusted by adding 0,01 M HCl or NaOH solution before adsorption experiment. The general procedure for both compounds was performed as follows. Accurately weighted amounts of magnetic nanoparticles were added to a [Cr(HY)(H_2O)] and Cr(III) aqueous solution of known concentration prepared with ultra pure water. This time was considered the starting point of the experiment. The samples were placed on a mini rotator at room temperature (24ºC). Supernatants were collected for analysis at known times, and the magnetic nanoparticles were separated using NdFeB magnet. The chromium equilibrium concentration was spectrophotometrically measured. Cr(III) ions were determined using atomic absorption spectrometry (**AAS**) and [Cr(HY)(H_2O)] complex equilibrium concentration was measured using a standard procedure based on the measurement of the absorbance at λ=544 nm.

The amount of Cr(III) ions and [Cr(HY)(H_2O)] complex adsorbed into the nanoparticles at time *t* (q_t, mg/g) was calculated by using the following expression:

$$q_t = (C_0 - C_t) \times \frac{V}{m} \qquad (5)$$

where C_0 (mg/L) is the initial concentration of Cr(III) or [Cr(HY)(H_2O)], C_t is the concentration at time *t* (mg/L), *V* is the total volume (L) and *m* is the mass of the dried nanoparticles (g) used as sorbent.

2.7.1 The effect of the pH on [Cr(HY)(H_2O)] complex

In order to determine the effect of the pH on the complex, a potentiometric titration of a solution of the [Cr(HY)(H_2O)] complex with NaOH was carried out. For this purpose prepared 50 mL of a solution of the complex with a concentration 0,005 M was prepared usng as a solvent a solution of 0,2 M KCl. During titration 50 mL of 0,02 M NaOH were

added. Value of pH solution of the complex before and after addition of NaOH was 2,38 and 11,65, respectively.

2.7.2 Kinetic experiments

The time profile of above compounds adsorption onto magnetic nanoparticles was assessed in order to investigate the kinetics of adsorption. For this purpose, 10 mg of Fe_3O_4@SiO_2-NH_2 and Fe_3O_4@SiO_2-NH_2-ALG (accurately weighted) were added to the aqueous solution of [Cr(HY)(H_2O)] complex (20 mL, 300 mg/L) and Cr(III) (20 mL, 30 mg/L), respectively. The pH of solutions was previously adjusted to 6. The solutions were shaken at room temperature (24ºC) and after 15 min, 30 min, 45 min, 1 h, 2 h, 3 h, 4 h, 8 h, 24 h and 48 h 1 mL of aliquots were collected. The amount of complex and Cr(III) ions adsorbed onto the magnetic nanoparticles at each time interval (q_t, mg/g) was determined and plotted against time (*t*, min) for kinetic modelling.

2.7.3 Equilibrium isotherms experiments

To obtain equilibrium isotherms *ca.* 1,5 mg (accurately weighted) of coated magnetic nanoparticles were dispersed in 3 mL solution. Initial concentration for [Cr(HY)(H_2O)] complex was 50, 100, 200, 300, 400 and 500 mg/L but for Cr(III) ions the initial concentration was 5, 10, 30, 50, 75 and 100 mg/L, both at pH=6.. The experiments were conducted at 24ºC for a total period of 24 h and for 8 h for [Cr(HY)(H_2O)] and Cr^{3+}, respectively. The amount of complex and Cr(III) ions adsorbed at equilibrium (q_e, mg/g) was assessed by UV-Vis spectroscopy for [Cr(HY)(H_2O)] and AAS for Cr(III). The calculations were performed using equation (5) for C=C_e.

2.8 Kinetics modelling

An analysis of the kinetic data is important because the kinetics describe the uptake rate of adsorbate, which in turn controls the resident time in the adsorbent-solution interface. To describe adsorption data two kinetic models, the pseudo-first-order (equation 6) and the pseudo-second-order equations (equation 7) [58] were used

$$q_t = q_e\left(1 - e^{-k_1 t}\right) \qquad (6)$$

$$q_t = \frac{k_2 q_e^2 t}{1 + k_2 q_e t} \qquad (7)$$

In these equations k_1 (h^{-1}) is the pseudo-first-order rate constant and k_2 ($g \cdot mg^{-1}h^{-1}$) is the of pseudo-second-order rate constant. The pseudo-first-order equation has been used to calculate the adsorption of solutes from liquid solutions in systems near equilibrium and in systems with a time independent solute concentration or linear behavior in equilibrium adsorption isotherms [64]. The pseudo-second-order kinetic equation is the opposite of previous model, because the second one usually predicts the behavior over the whole range of adsorption [65].

2.9 Isotherm modelling

Equilibrium data are the basic requirements for the design of adsorption systems and provide valuable information to assess the adsorption capacity of an adsorbent. Also give and understanding on the interactions between the adsorbate and the adsorbent, at equilibrium under isothermal conditions [70]. Many isotherm equations are commonly used, including Langmuir, Freundlich, Redlich-Peterson, Temkin and Elovich. In this work, the equilibrium adsorption data of Cr(III) ions and [Cr(HY)(H2O)] has been investigated using the Langmuir and Freundlich isotherm models.

The first one is based on the assumption that all sites possess equal affinity for the adsorbate and a monolayer is formed when the solid surface reaches saturation [66]. The mathematical expression shows equation (8) and the linear expression (9)

$$q_e = \frac{q^0 K_L C_e}{1 + K_L C_e} \qquad (8)$$

$$\frac{C_e}{q_e} = \frac{1}{K_L q^0} + \frac{C_e}{q^0} \qquad (9)$$

where q^0 *is the* Langmuir monolayer adsorption capacity (mg/g), K_L is the Langmuir isotherm constant (L/mg) and q_e (mg/g) and C_e (mg/L) are the amount of adsorbate adsorbed and the final adsorbate concentration in solution at equilibrium, respectively.

The Freundlich isotherm model is an empirical equation based on heterogenous surfaces suggesting that binding sites are not equivalent and/or independent which is given as:

$$q_e = K_F (C_e)^{\frac{1}{n}} \qquad (10)$$

$$\ln q_e = \ln K_F + \frac{1}{n}(\ln C_e) \qquad (11)$$

Where K_F Freundlich isotherm constant [(mg/g)(L/mg)(1-n/n)] and n Freundlich exponent (dimensionsless) related to adsorption capacity and adsorption intensity, respectively

3. Results and discussion

3.1 Characterization of magnetic nanoparticles

Magnetic iron oxide nanoparticles were synthesized by oxidative hydrolysis of iron(II) sulphate in alkaline conditions and under an atmosphere of N_2. KOH and KNO_3 were first heated and then an aqueous solution of $FeSO_4 \cdot 7H_2O$ was added to the mixture. Reaction of this synthesis is shown in equation 12.

$$6Fe^{2+} + SO_4^{2-} + 18OH^- \xrightarrow{N_2,\Delta} 2Fe_3O_4 \downarrow + SO_3^{2-} + 9H_2O \quad (12)$$

To confirm the crystal structure of the magnetite, XRD experiment was performed and the resulting difractogram is shown in figure 16. According to the literature [68, 69, 70], the lattice spacing calculated from the diffraction peaks observed at 30º, 35º, 37º, 43º, 53º, 57º and 62º matched the [220], [311], [222], [400], [422], [511] and [440] planes of Fe_3O_4 crystals, respectively. These results suggest that the main crystalline phase obtained is magnetite (Fe_3O_4).

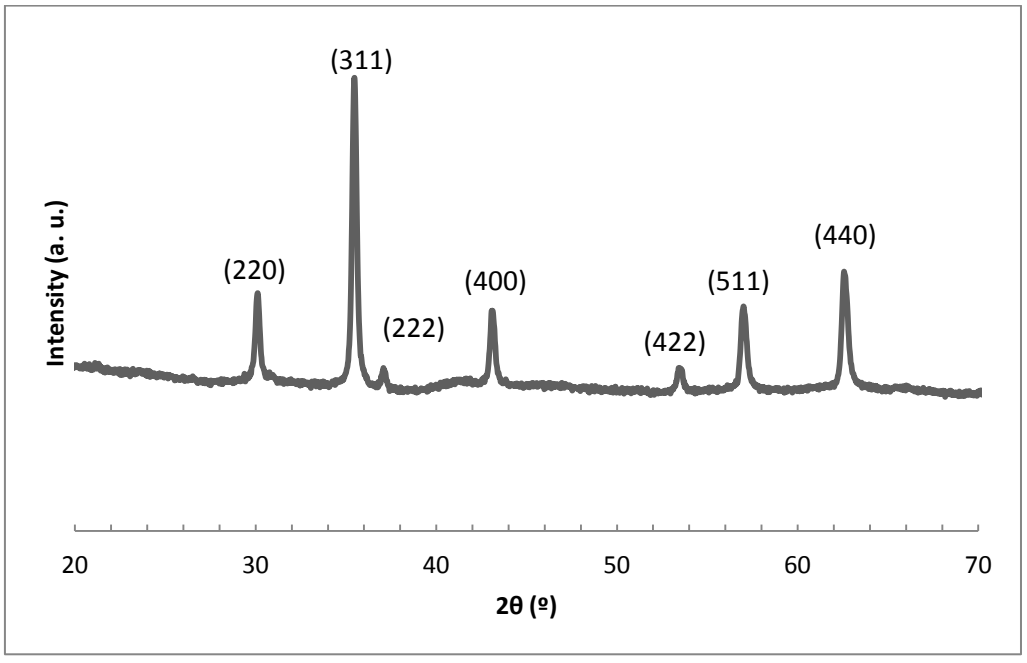

Figure 13. X-ray diffraction patterns of Fe_3O_4

The Fe3O4 nanoparticles are spheroidal with an average particle diameter of 55 nm, as seen by scanning electron microscopy (SEM) in figure 14.

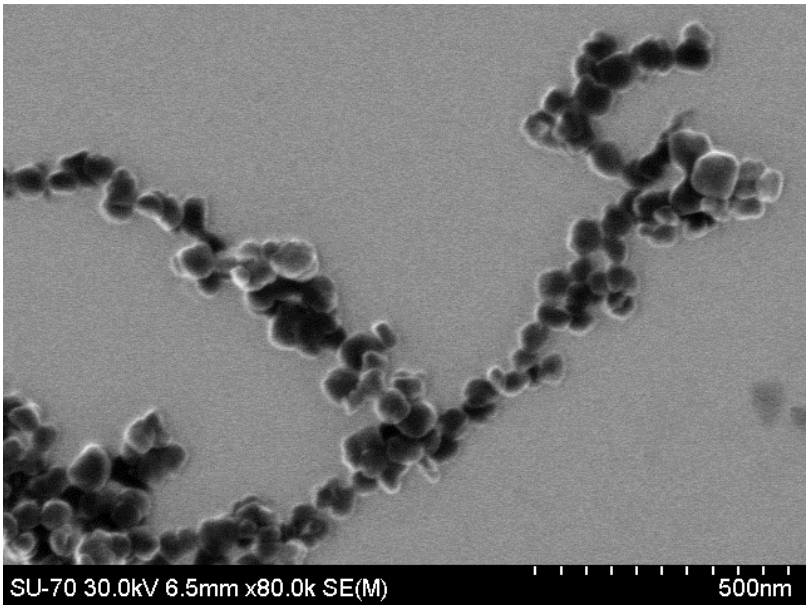

Figure 14. SEM micrograph of Fe_3O_4 nanoparticles (courtesy: Dr. Ana Estrada, University of Aveiro)

Prepared magnetic nanoparticles, as described above, were coated with amorphous silica shell functionalized with amine groups. This reaction was performed by hydrolysis of TEOS in alkaline conditions with ammonia solution acting as a catalyst. The surface amino modification of the silica coated magnetite was performed via hydrolysis and condensation of APTMS. Equations 13 and 14 show chemical reactions described above.

$$Si(OC_2H_5)_4 + 2H_2O \xrightarrow{NH_3} SiO_2 + 4C_2H_5OH \qquad (13)$$

$$Fe_3O_4 + SiO_2 \rightarrow \text{OH OH OH nanoparticle} \qquad (14)$$

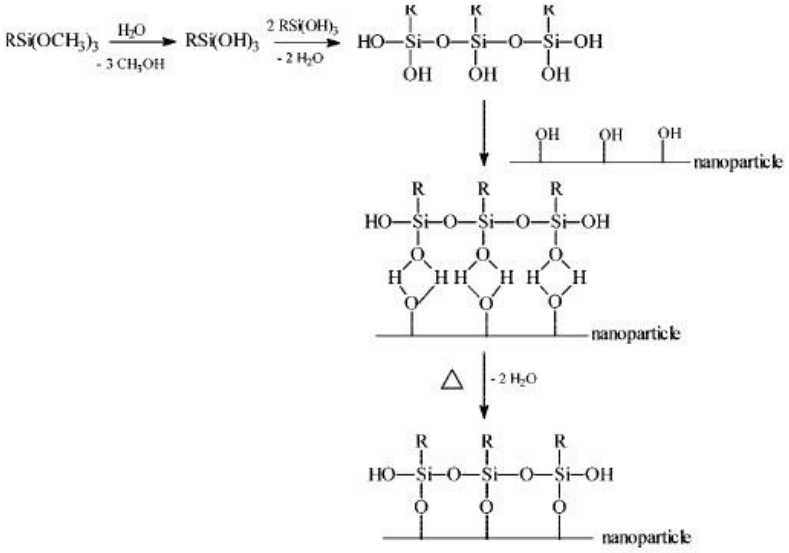

Figure 15. Reactions of chemical modified of magnetic nanoparticles (R= $-(CH_2)_3-NH_2$)

Covalent attachment of alginate to the particles coated with amorphous silica shell functionalized with amine groups was carried out using EDC and NHS. The reaction between $–NH_2$ groups of the surface of the particles with silica shell and the –COOH groups of the alginate is achieved by carbodiimide activation, using above compounds. Figure 16 shown the structure of the new nanoparticle obtained above method.

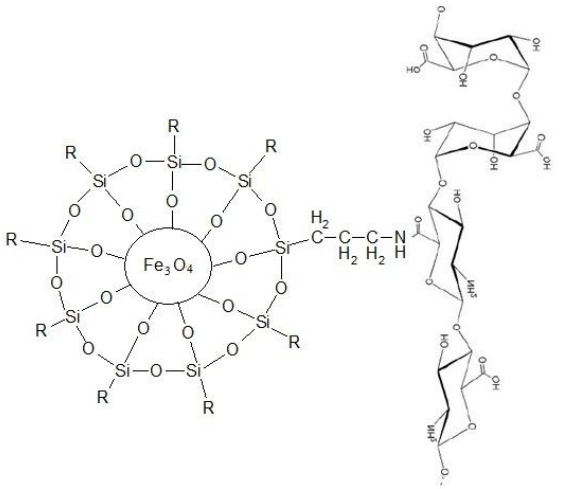

Figure 16. Structure of the new nanoparticle covalent attachment of alginate $Fe_3O_4@SiO_2$-NH_2-ALG

Figure 17 shows Fourier transform infrared (FT-IR) spectra of the iron oxide nanoparticles (Fe_3O_4), iron oxide nanoparticles coated with silica shell functionalized with amine groups (Fe_3O_4@SiO_2-NH_2) and after covalent linkage with alginate (Fe_3O_4@SiO_2-NH_2-ALG). The spectra of magnetite show strong bands in the low-frequency region (1000-400 cm^{-1}) due to the iron oxide skeleton [66]. The characteristic band of ν(Fe-O) is at 579cm^{-1} in the FT-IR spectrum. The formation of a silica-coating on the magnetite surface was confirmed by bands at 1124 cm^{-1}, 1052 cm^{-1}, 779 cm^{-1} and 455cm^{-1} assigned to the Si-OH vibration, Si-O-Si and Fe-O-Si groups [67]. The peak at 3421 cm^{-1} is attributed to the O-H stretching vibrations of the hydroxyl group on the surface of silica [68]. Successful amino-functionalization of the silica layer on magnetite surface was confirmed by the absorption bands at 1635 cm^{-1}, 1558 cm^{-1}, 1496 cm^{-1}. These bands ascribed to the N-H stretching and bending vibrations of amino groups. The FT-IR spectrum of magnetite with alginate show bands at 1632 cm^{-1} attributed to the antisymmetric stretch of ν_{as} (COO^-) and 1413 cm^{-1} attributed to the symmetric stretch ν_s(COO^-) which corroborate the presence of the polysaccharide alginate.

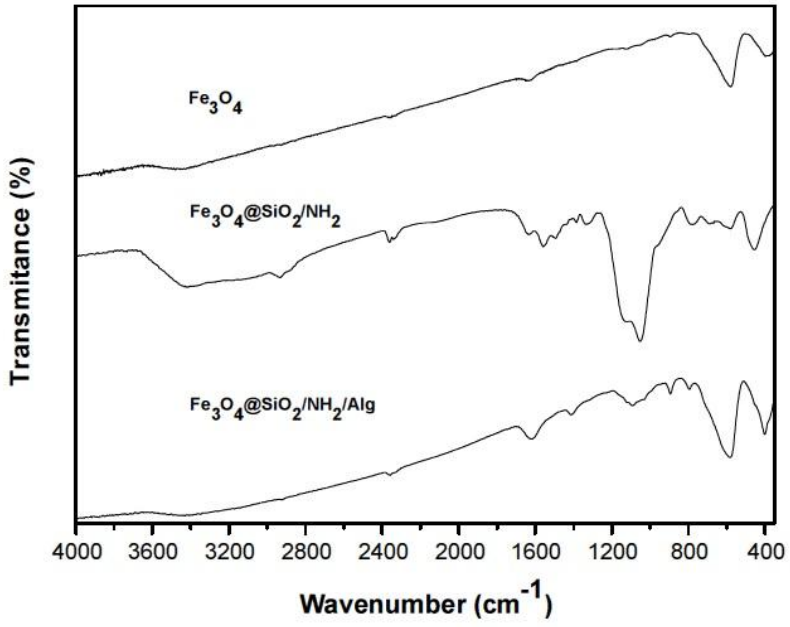

Figure 17. FT-IR spectra of (a) Fe_3O_4 (b) Fe_3O_4@SiO_2-NH_2 (c) Fe_3O_4@SiO_2-NH_2-ALG

Table 5 presents the experimental values of C, H and N percentage of Fe_3O_4, Fe_3O_4@SiO_2-NH_2 and Fe_3O_4@SiO_2-NH_2-ALG measured by elemental analysis. The highest percentage of N appears in sample Fe_3O_4@SiO_2-NH_2, which confirms the presence of amine groups. After the covalent linkage with the alginate the C percentage increases significantly which may be a proof of the presence of alginate in the last sample. Thus this technique allowed to confirm the successful coating of magnetite nanoparticles with amorphous silica shell functionalized with amine groups and the attachment of alginate to the magnetic nanoparticles.

Table 5. Results of elemental analysis of the nanoparticles.

Sample	% C	% H	% N
Fe_3O_4	0,1247	0,1263	-
Fe_3O_4@SiO_2-NH_2	1,0948	0,4464	0,3998
Fe_3O_4@SiO_2-NH_2-ALG	2,2449	0,6579	0,3768

The modification of the surface of Fe_3O_4 nanoparticles was further confirmed by thermogravimetric analysis (TGA). Figure 18 compares the TGA curves of the several samples. It can be seen that the weight loss of the Fe_3O_4 is much higher than the Fe_3O_4@SiO_2-NH_2 and the Fe_3O_4@SiO_2-NH_2-ALG. This may be caused by the presence of contamination of magnetite.

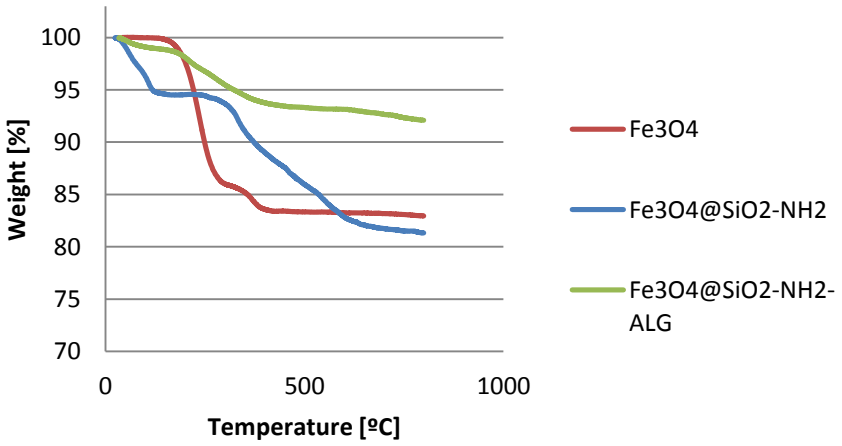

Figure 18. TGA graphs of Fe_3O_4; Fe_3O_4@SiO_2-NH_2 and Fe_3O_4@SiO_2-NH_2-ALG

The nanoparticles prepared in this work were magnetic as they could be collected by using an NdFeB magnet. A detailed characterization of the magnetic properties of the nanoparticles here investigated was not carried out. However previous studies performed in the same laboratory in similar magnetic samples have confirmed the magnetic properties of magnetic nanoparticles. For instance Girginowa et al. [15] performed magnetic measurements for Fe_3O_4 nanoparticles with an average size of 80 nm and $Fe_3O_4@SiO_2$ samples at T=293 K. In these magnetometric measurements the sample is exposed to an external magnetic field and the magnetization is recorded with a magnetometer. Uncoated particles shown high values of magnetization saturation (92 $emu \cdot g^{-1}$, 90 $emu \cdot g^{-1}$) that decreases after silica coating. Both exhibited coercivity and remanent magnetization. The saturation magnetization has decreased with the modification of the pure magnetite while the coercivity has increased. Similar research has been studied by Goya et al. [69]. Magnetic properties were confirmed also by Salgueiro et al. [70], but in this case magnetic measurements were performed for bare and carrageenan coated magnetic nanoparticles with an average diameter of 20 nm at T=300 K. Values of magnetization saturation show that after polymer coating the magnetization saturation decreases to approximately half of the initial value.

The surface charge of the nanoparticles $Fe_3O_4@SiO_2$-NH_2 and $Fe_3O_4@SiO_2$-NH_2-ALG was assessed by zeta potential measurements. This is important to confirm the potential application of these nanoparticles for the removal of chromium(III) complex with EDTA and Cr(III) ions, used zeta potential measurements. These measurements were performed at variable pH and the results are presented in table 6.

Table 6. Values of Zeta potential obtained in ultra pure water at variable pH

Sample	pH	Zeta Potential [mv]
$Fe_3O_4@SiO_2$-NH_2	4,66	5,71 ± 1,80
	5,14	2,30 ± 0,35
	6,24	5,69 ± 0,87

	7,31	-26,8 ± 0,30
	8,23	-21,23 ± 1,0
Fe3O4@SiO2-NH2-ALG	4,03	-35,53 ± 1,78
	5,42	-41,83 ± 2,08
	6,27	-40,50 ± 0,50
	7,86	-50,47 ± 1,20
	8,06	-53,27 ± 2,75

In aqueous media the pH of the samples is one of the most important factors that affect its zeta potential. Is visible that if more alkali is added to the solution then the particles tend to aquire more negative charge, and is opposite way is when acid is added to the solution. Therefore, a zeta potential versus pH curve is positive at low pH and negative at high pH. In the case of Fe_3O_4@SiO_2-NH_2 was expected positive charge, due to –NH_2 group, but for Fe_3O_4@SiO_2-NH_2-ALG, negative charge, due to COO^- groups of alginate. Zeta potential measurements revealed a positive and negative surface charge for

the above nanomaterials. In pH 6 these values were 5,69 and -40,50 mV for nanoparticles with amine groups and with alginate, respectively.

3.2 Adsorption experiments

3.2.1 Uptake of [Cr(HY)(H_2O)] complexes using Fe_3O_4@SiO_2-NH_2 particles

3.2.1.1 The effect of pH on [Cr(HY)(H_2O)] complex

[Cr(HY)(H_2O)] complex is composed of Cr(III) ion, an water molecule and EDTA anion, which in this case is present in the HY^{3-} form, where Y^{4-} represents the EDTA molecule totally deprotonated (Figure 19).

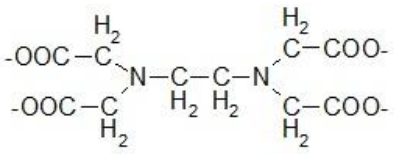

Figure 19. Chemical structure of Y^{4-} anion

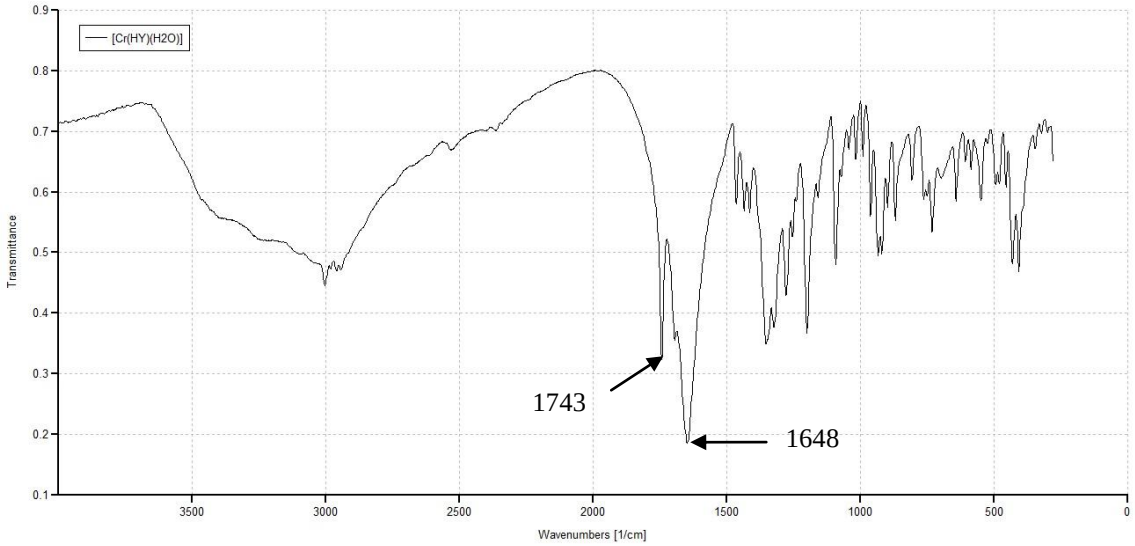

Figure 20. FTIR spectrum of the complex [Cr(HY)(H_2O)]

Figure 20 shows the FTIR spectrum of the complex [Cr(HY)(H_2O)] presenting intense peaks. A strong band appears at 1743 cm^{-1} and can be assigned to the non-ionized and uncoordinated COO stretching band. The vibration band of the ionized and coordinated COO- appears at 1650-1590 cm^{-1}, but for coordination to metal ions such as Cr(III) it occurs at 1648 cm^{-1}.

In aqueous solution the complex [Cr(HY)(H_2O)] behaves like a diprotic acid, due to the arrangement of ligands, which is shown in equations 15 and 16.

$$[Cr(HY)(H_2O)] + H_2O \Leftrightarrow [Cr(Y)(H_2O)]^- + H_3O^+ \quad (15)$$

$$[Cr(Y)(H_2O)]^- + H_2O \Leftrightarrow [Cr(Y)(OH)]^{2-} + H_3O^+ \quad (16)$$

The first form of the complex ([Cr(HY)(H_2O)]) is purple, but the second ($[Cr(Y)(OH)]^{2-}$) is blue and thus it is relatively easy to recognize which form exists at a specific pH value. With this purpose, the potentiometric titration of an acid solution of the complex using NaOH(aq) as a titrant was carried out The graphical representation of the pH value versus the volume of base added is shown in figure 21. Two equivalence points are visible. Before the first point solution is still acidic, so the equilibrium concentration of $[Cr(Y)(OH)]^{2-}$ is negligible. The first equivalence point in the graph is attributed to the formation of $[Cr(Y)(H_2O)]^-$, while the second point is assigned to the formation of the blue compound $[Cr(Y)(OH)]^{2-}$ [72].

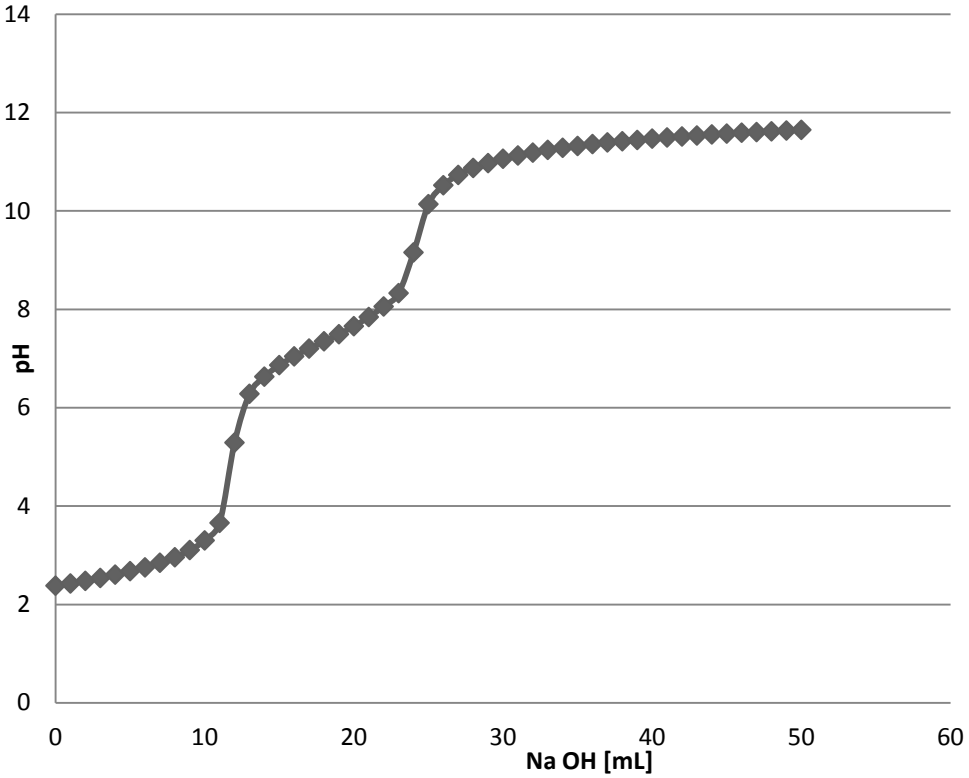

Figure 21. Potentiometric titration curve of [Cr(HY)(H_2O)] with NaOH

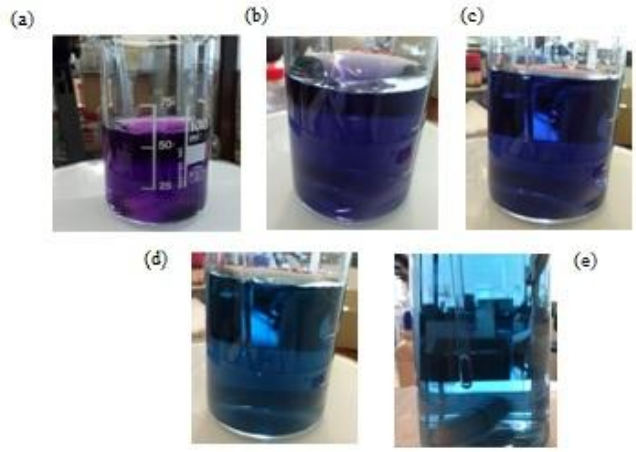

Figure 22. Color of the solution at different pHs (a) 2,38 (b) 7,66 (c) 8,06 (d) 11,24 (e) 11,55

3.2.1.2 Kinetic studies

The time profile of the [Cr(HY)(H_2O)] uptake by the nanoparticles coated with amorphous silica shell functionalized with amine groups, for initial concentration of complex (300 mg/L) at 24ºC is present in figure 23. Is visible that the adsorption curve displays an usual shape. A rapid adsorption takes place at the beginning and after 24 h decreases. Figure 23 represents the concentration of the complex that remains in solution with time. As is shown in figure, on the beginning concentration reached variable values, but after 4 hours is visible decrease of the concentration. These different values may be due to errors during experiment or during characterization of samples. As was written previous, the magnetic nanoparticles were separate magnetically and then the supernatant were analyzed by UV-VIS spectroscopy. Due to the dark color of the nanoparticles, they absorb the radiation so, even residual amount of nanoparticles, may affect to final calculations. Therefore, the concentration of [Cr(HY)(H_2O)] complex has unusual values.

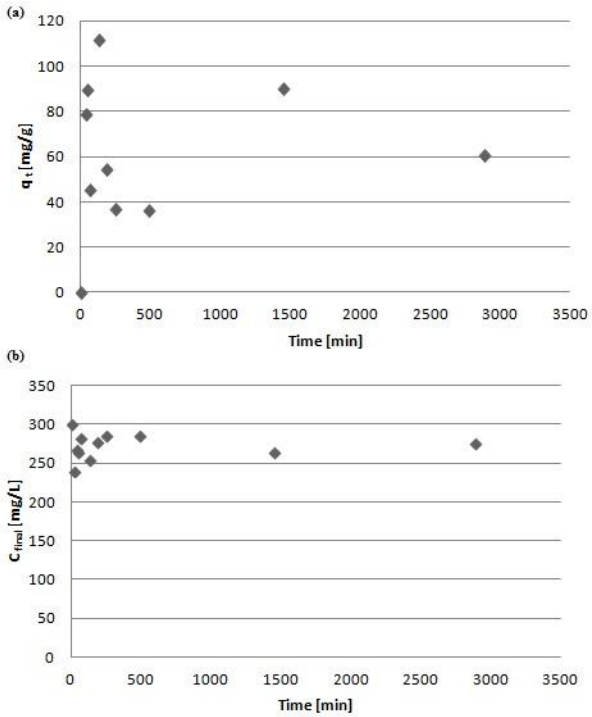

Figure 23. The time profile of the [Cr(HY)(H_2O)] uptake by Fe_3O_4@SiO_2-NH_2 (a) concentration of complex in aqueous solution (b)

The adsorption kinetics was investigated and the experimental data was fitted with well-known kinetic models such as the pseudo-first-order and the pseudo-second-order kinetic equation, given by equation (6) and (7), respectively. Table 7 shows kinetic parameters obtained using both models. The results show that both models describe not well the kinetics of [Cr(HY)(H_2O)] complex removal. To compare both models, the pseudo-second-order model describe better the kinetic of complex removal as confirmed by the higher value of R^2 (table 7).

Table 7. Kinetic parameters estimated from pseudo 1st and 2nd order equations and evaluations of its fittings

Model	Parameters	R^2
Pseudo-1st order	q_e (mg/g) 31,7852	0,0055
	k_1 (h^{-1}) $1 \cdot 10^{-4}$	
Pseudo-2nd order	q_e (mg/g) 64,5161	0,954
	k_2 ($g \cdot mg^{-1} \cdot h^{-1}$) $0{,}4820 \cdot 10^{-4}$	

3.2.1.3 Isotherm studies

A plot of the solute concentration in the adsorbent phase q_e (mg/g) as function of the solute concentration in the solution C_e (mg/L) at equilibrium gives an adsorption isotherm (figure 24). As shown the figure 24 adsorption capacity decrease with increasing of concentration of [Cr(HY)(H_2O)] complex. This indicates that the [Cr(HY)(H_2O)] complex are adsorbed onto the surface of the Fe_3O_4@SiO_2-NH_2 particles.

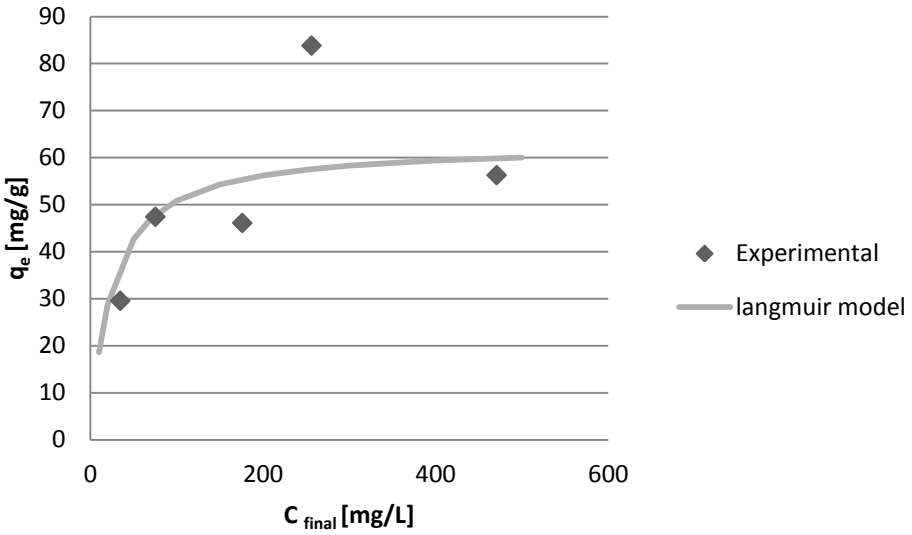

Figure 24. Isotherm of the adsorption of [Cr(HY)(H_2O)] using Fe_3O_4@SiO_2-NH_2 nanoparticles (a) fit of Langmuir isotherm model for adsorption of above complex

In order to understand and clarify the adsorption process, Langumir adsorption isotherm and Freundlich adsorption isotherm models were applied in this study. The isotherm constants were calculated from the experimental data and presented in table 8. Taking into consideration the values of the correlation coefficient as a criterion for goodness of fit for the system, the Langumir isotherm model (figure 24) shows better correlation (R^2=0,9191) than the Freundlich adsorption isotherm model. The adsorption data confirm that the Langumir isotherm can be interpreted as indicating a homogeny adsorption process, leading to monolayer binding.

Table 8. Langumir and Freundlich isotherm model parameters for adsorption [Cr(HY)(H_2O)] complex

Langmuir isotherm model			**Freundlich isotherm model**		
q^0 (mg·g^{-1})	K_L (L·mg^{-1})	R^2	K_F ((mg/g)·(mg/L)^n)	n	R^2
62,9	0,042	0,9191	12,1	3,51	0,6062

3.2.2 Uptake of Cr(III) species using Fe_3O_4@SiO_2-NH_2-ALG particles

3.2.2.1 Kinetic studies

The adsorption of Cr(III) species, with initial concentration 30 mg/L, by Fe_3O_4@SiO_2-NH_2-ALG particles as a function of the contact time is shown in figure 25 a. It shows that the plots are not linear over the whole time range which confirm that Cr(III) species were adsorbed. Also is shown that the adsorption capacity increases with increasing contact time. The figure 25 b presents changing of concentration with time. Is shown that concentration of Cr(III) decreases with increasing contact time, so this may indicate that magnetic nanoparticles with covalent attachment of alginate are able to remove of Cr(III) species from aqueous solution.

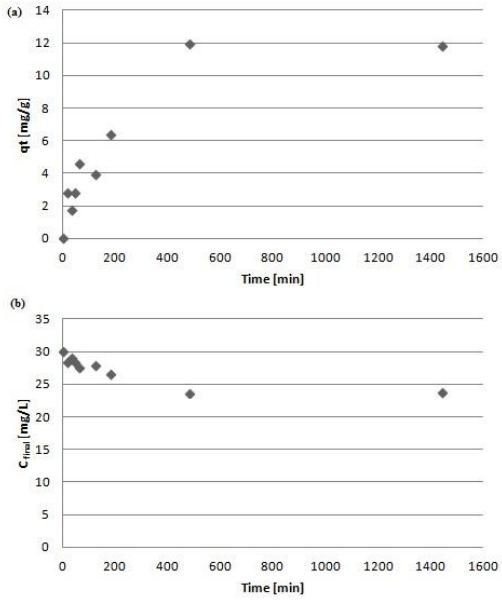

Figure 25. The time profile of adsorption capacity of Cr(III) species onto Fe_3O_4@SiO_2-NH_2-ALG (a) Change in the concentration of Cr(III) vs time (b)

Table 9 lists the kinetics constants evaluated from the adsorption kinetics, along with the correlation coefficients and the experimental adsorption capacities.The pseudo-first-order model and the pseudo-second-order model fit equally because R^2 is similar in both cases.

Table 9. Kinetic parameters estimated from pseudo 1st and 2nd order equations and evaluations of its fittings

Model	Parameters	R^2
Pseudo-1st order	q_e (mg/g) 9,7796	0,965
	k_1 (h^{-1}) 0,0033	
Pseudo-2nd order	q_e (mg/g) 12,9199	0,966
	k_2 ($g \cdot mg^{-1} \cdot h^{-1}$) $6{,}01 \cdot 10^{-4}$	

3.2.2.2 Isotherms

Figure 26 shows the adsorption isotherm curves present isotherms of Cr(III) on Fe_3O_4@SiO_2-NH_2-ALG particles in aqueous solution. The isotherm curves present the Cr(III) uptake as a function of the equilibrium Cr(III) solution concentration at room temperature. It can be seen that in the beginning the adsorption capacity decreases, which may be the result of errors during characterization of solution after the experiment. After this point the adsorption capacity increases and the graph resume normal shape. This behavior may prove that magnetic nanoparticles can be employed to removal Cr(III) species from water.

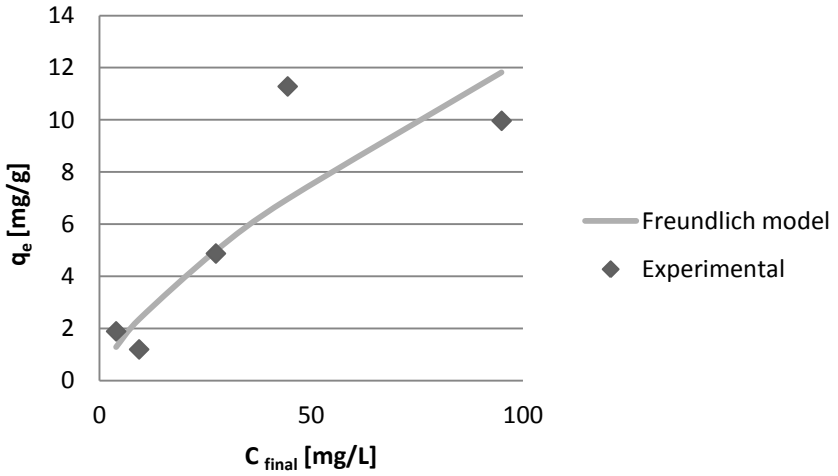

Figure 26. Isotherm of the adsorption of Cr(III) using Fe_3O_4@SiO_2-NH_2-ALG nanoparticles and fit of Freundlich isotherm model for adsorption of above complex

The Langmuir and Freundlich isotherm models parameters for Cr(III) ions obtained from the fitting of experimental data are listed in table 10. The results in table 10 suggested that Freundlich isotherm model (figure 26) describes the adsorption of metal ions better than of Langmuir model, evidenced by higher R^2. Values of *n* implies stronger interaction between adsorbent and metal and also is in the range of $1<n<10$, which also demonstrates that these particle act as a favorable adsorbent for the removal of Cr(III) from aqueous solution. Nevertheless, the R^2 obtained for the Freundlich model fitting was still low, which indicates that both models do not describe the adsorption capacity satisfactory.

Table 10. Langmuir and Freundlich isotherm model parameters for adsorption Cr(III) species

Langmuir isotherm model			**Freundlich isotherm model**		
q^0 (mg·g^{-1})	K_L (L·mg^{-1})	R^2	K_F ((mg/g)·(mg/L)^n)	n	R^2
19,8019	0,01266	0,3863	0,4934	1,4337	0,781

4. Conclusion and perspectives of future work

Magnetite nanoparticles coated with an amorphous silica shell functionalized with amine groups were prepared and evaluated as magnetic sorbents for the removal of Cr(III) EDTA complexes, here designated as [Cr(HY)(H_2O)], from aqueous solutions, using simple NdFeB magnet. Under the experimental conditions used (pH=6, room temperature), the nanoparticles showed affinity for the complex and allowed its removal . The adsorption followed a pseudo-second order kinetics, while the equilibrium adsorption was better described by the Langmuir isotherm model, that estimated a maximum adsorption capacity of 62 mg/g.

The biopolymer alginate was successfully covalently attached to the amine surface functionalized nanoparticles, to our knowledge for the first time. The reaction between the –NH_2 groups of the surface of the particles Fe_3O_4@SiO_2-NH_2 and the –COOH groups of the alginate was achieved by carbodiimide activation, using EDC and NHS. The resulting nanoparticles were employed to uptake Cr(III) species from aqueous solutions. The adsorption kinetics was well described by both pseudo-first and pseudo-second order equations. For the isotherm studies, the Freundlich model gave better results than the Langmuir model, although still unsatisfactory due to low R^2.Results described in this work indicate that these particles can be used for Cr(III) species removal from aqueous solution.

To assess the full potential of the materials here developed for the uptake of Cr(III) species from water, additional studies are necessary for the evaluation of optimal uptake conditions, such as initial concentration, pH and temperature, as well as the study of the kinetics and equilibrium isotherms for the removal of different metal cations, and the evaluation of their performance in the purification of real effluents of different chemical composition.

Reference

[1] Khajeh M., Laurent S., Dastafkan K., *Nanosorbents: classification, preparation, and applications (with emphasis on aqueous media)*, Chemical Reviews (2012)

[2] Lopez-Serrano A., Munoz Olivas R., Sanz Landaluze J., Camara C., *Nanoparticles: a global vision. Characterization, separation, and quantification methods. Potential environmental and health impact*, Analytical Methods 6 (2014) 38-56

[3] Liu Y., Liang P., Guo L., *Nanometer titanium dioxide immobilized on silica gel as sorbent for preconcentration of metal ions prior to their determination by inductively coupled plasma atomic emission spectrometry,* Talanta 68 (2005) 25-30

[4] Mohmood I., Lopes C., Lopes I., Ahmad I., Duarte A., Pereira E., *Nanoscale materials and their use in water contaminants removal- a review,* Environmental Science and Pollution Research 20 (2013) 1239-1260

[5] Zhang L., Fang M., *Nanomaterials in pollution trace detection and environmental improvement,* Nano Today 5 (2010) 128-142

[6] Wigginton N., Haus K., Hochella M., *Aquatic environmental nanoparticles,* Jurnal of Environmental Monitoring 9 (2007) 1285-1432

[7] Kroto H. W., Heath J.R., O'Brien S. C., Curl R. F., Smalley R. E., *C_{60}: Buckminsterfullerene,* Nature 318 (1985) 162-163

[8] Elyasi P., SalmanOgli A., *Investigation of potential profile effects in quantum dot and onion- like quantum dot-quantum well on optical properties,* Optics Communications 318 (2014) 26-30

[9] Ferreira da Silva B., Perez S., Gardinalli P., Singhal R., Mozeto A., Barcelo D., *Analytical chemistry of metallic nanoparticles in natural environments,* Trends in Analytical Chemistry 30 (2011) 528-540

[10] Gubin S., Koksharov Y., Khomutov G., Yurkov G., *Magnetic nanoparticles: preparation, structure and properties,* Russian Chemical Reviews 74 (2005) 489-520

[11] Poole Ch., Owens F., *Introduction to nanotechnology,* Wiley Interscience, (2003), Chapter 7

[12] Jiles D., *Introduction to magnetism and magnetic materials,* Taylor & Francis Group, Chapter 4

[13] Cornell R., Schwertmann U., *The iron oxides structure, properties, reactions, occurrences and uses,* Wiley-Vch (2000)

[14] Cademartiri L., Ozin G., *Concepts of nanochemistry,* Wiley-Vch (2009) Chapter 6

[15] Girginova P., Daniel-da-Silva A., Lopes C., Figueira P., Otero M., Amaral V., Pereira E., Trindade T., *Silica coated magnetite particles for magnetic removal of Hg^{2+} from water,* Journal of Colloid and Interface Science 345 (2010) 234-240

[16] Suleiman J., Hu B., Peng H., Huang Ch., *Separation/preconcentration of trace amounts of Cr, Cu and Pb in environmental samles by magnetic solid-phase extraction with Bismuthiol-II-immobilized magnetic nanoparticles and their determination by ICP-OES,* Talanta 77 (2009) 1579-1583

[17] Chen L., Wang T., Tong J., *Application of derivatized magnetic materials to the separation and the preconcentration of pollutants in water samples,* Trends in Analytical Chemistry 30 (2011) 1095-1108

[18] Lu A., Salabas E., Schuth F., *Magnetic nanoparticles: synthesis, protection, functionalization and application,* Angewandte Chemie 46 (2007) 1222-1244

[19] Massart R., *Preparation of aqueous magnetic liquids in alkaline and acidic media,* 17 (1981) 1247

[20] Charles S., *The preparation of magnetic fluids,* Lecture Notes in Physics 594 (2002) 3-18

[21] Gubin S., Koksharov Yu., Khomutov G., Yurkov G., *Magnetic nanoparticles: preparation, structure and properties,* Russian Chemical Reviews 74 (2005) 489-520

[22] Wang Y., Yang H., *Synthesis of iron oxide nanorods and nanocubes in an imidazolium ionic liquid,* Chemical Engineering Journal 147 (2009) 71-78

[23] Jiao H., Wang J., *Thermal decomposition fabrication, growth mechanism and characterization of Rod-Like γ-Fe_2O_3,* Metal-Organic and Nano-Metal Chemistry 44 (2014) 1354-1357

[24] Butter K., Philipse A., Vroege G., *Synthesis and properties of iron ferrofluids,* Journal of Magbetism and Magnetic Materials 252 (2002) 1-3

[25] Carlos L., Garcia Einschlag F., Gonzalez M., Martire D., *Applications of megnetite nanoparticles for heavy metal removal from wastewater,* ISBN 978-953-51-0882-5 (2013) Chapter 3

[26] Langevin D., *Micelles and microemulsions,* Annual Review of Physical Chemistry 43 (1992) 327-349

[27] Paul B., Moulik S., *Uses and applications of microemulsions,* Current Science 80 (2001) 990-1001

[28] Gupta A., Gupta M., *Synthesis and surface engineering of iron oxide nanoparticles for biomedical applications,* Biomaterials 26 (2005) 3995-4021

[29] Laurent S., Forge D., Port M., Roch A., Robic C., Elst L., Muller R., *Magnetic Iron Oxide Nanoparticles: Synthesis, stabilization, vectorization, physicochemical characterizations, and biomedical applications,* Chemical Review 108 (2008) 2064-2110

[30] Yang S., Paik S., Ryu J., Choi K., Kang T., Lee J., Song Ch., Ko S., *Dynamic light scattering- based method to determine primary particle size of iron oxide nanoparticles in simulated gastrointestinal fluid,* Food Chemistry 161 (2014) 185-191

[31] Lim J., Yeap S., Che H., Low S., *Characterization of magnetic nanoparticle by dynamic light scattering,* Nanoscale research letters 8 (2013) 1-14

[32] Zhou W., Apkarian R., Wang Z., Joy D., *Fundamentals of Scanning Electron Microscopy,* Scanning Microscopy for Nanotechnology (2007) 1-40

[33] Chorupa I., Douziech-Eyrolles L., Nagaboini-Okassa L., Fouquenet J., Cohen-Jonathan S., Souce M., Marchais H., Dubois P., *Molecular composition of iron oxide*

nanoparticles, precursors for magnetic drug targeting, as characterized by confocal Raman microspectroscopy, Analyst 130 (2005) 1395-1403

[34] Russo P., Acierno D., Palomba M., Carotenuto G., Rosa R., Rizzuti A., Leonelli C., *Ultrafine magnetite nanopowder: Synthesis, characterization and preliminary use as filler of polymethylmethacrylate nanocomposites,* Jurnal of Nanotechnology 2012 (2012) 1-8

[35] Bajpai A., Gupta R., *Evaluation of water sorption behavior and In Vitro blood compatibility of polyvinyl alcohol based magnetic bionanocomposites,* Journal of Applied Polymer Science 114 (2009) 3548-3560

[36] Ruiz-Hitzky E., Darder M., Aranda P., *Functional biopolymer nanocomposites based on layered solids,* Journal of Materials Chemistry 15 (2005) 3650-3662

[37] Aime C., Coradin T., *Nanocomposites from biopolymer hydrogels: blueprints for white biotechnology and green materials chemistry,* Journal of polymer science 50 (2012) 669-680

[38] Im S., Herricks T., Lee Y., Xia Y., *Synthesis and characterization of monodisperse silica colloids loaded with superparamagnetic iron oxide nanoparticles,* Cgemical physics letters 401 (2005) 19-23

[39] del Campo A., Sen T., Lellouche J., Bruce I., *Multifunctional magnetite and silica-magnetite nanoparticles: Synthesis, surface activation and applications in life sciences,* Journal of Magnetism and Magnetic Materials 293 (2005) 33-40

[40] Yamaura M., Camilo R., Sampaio L., Macêdo M., Nakamura M., Toma H., *Preparation and characterization of (3-aminopropyl)triethoxysilane- coated magnetite nanoparticles,* Journal of Magnetism and Magnetic Materials 279 (2004) 210-217

[41] Singh S., Barick K., Bahadur D., *Surface engineered magnetic nanoparticles for removal of toxic metal ions and bacterial pathogens,* Journal of hazardous materials 192 (2011) 1539-1547

[42] Chen J., Xing H., Guo H., Li G., Weng W., Hu S., *Preparation, characterization and adsorption properties of a novel 3-aminopropyltriethoxysilane functionalized sodium*

alginate porous membrane adsorbent for Cr(III) ions, Journal of Hazardous Materials 248-249 (2013) 285-294

[43] Araujo M., Teixeira J., *Trivalent chromium sorption on alginate beads,* International Biodeterioration & Biodegradation 40 (1997) 63-74

[44] Vassileva P., Detcheva A., Uzunov I., Uzunova S., *Removal of metal ions from aqueous solutions using pyrolyzed rice husks: adsorption kinetics and equilibria*, Chemical Engineering Communications 200 (2013) 1578-1599

[45] Rocha L., Lopes C., Borges J., Duarte A., Pereira E., *Valuation of unmodified rice husk waste as an eco-friendly sorbent to remove mercury: a study using environmental realistic concentrations,* Water air and soil pollution 224 (2013) 1-18

[46] Nakbanpote W., Thiravavetyan P., Kalambaheti C., *Comparison of gold adsorption by Chlorella vulgaris, rice husk and activated carbon,* minerals Engineering 15 (2002) 549-552

[47] Marshall W., Champagne E., Evans W., *Use of rice milling byproducts (hulls and bran) to remove metal ions from aqueous solution,* Journal of Environmental Science and Health 28 (1993) 1977-1992

[48] Fiol N., Serarols J., Poch J., Martinez M., Miralles N., Villaescusa I., *Low cost materials for metal uptake from aqueous solutions,* Environmental Chemistry, Chapter 24 (2005) 251-258

[49] Sidiras D., Politi D., batzias F., Boukos N., *Efficient removal of hexavalent chromium from aqueous solutions using autohydrolyzed Scots Pine (Pinus Sylvestris) sawdust as adsorbent,* International Journal of environmetal science and technology 6 (2013) 1337-1348

[50] Khosravihaftkhany S., Morad N., Teng T., Abdullah A., Norli I., *Biosorption of Pb(II) and Fe(III) from aqueous solutions using oil palm biomasses as adsorbents,* Water air and soil pollution 3 (2013) 1455

[51] Lavecchia R., Pugliese A., Zuorro A., *Removal of lead from aqueous solutions by spent tea leaves,* CISAP4: 4th international conference on safety & environment in process industry (2010) 73-78

[52] Abdel-Halim E., Al-Deyab, *Removal of heavy metals from their aqueous solutions through adsorption onto natural polymers,* Carbohydrate Polymers 84 (2011) 454-458

[53] Choong J., Nah I., Hwang K., *Adsorption of heavy metals using magnetically modified alginic acid,* Hydrometallurgy 86 (2007) 140-146

[54] Nayak D., Banerjee A., Roy S., Lahiri S., *Speciation dependent studies on chromium absorption using calcium alginate and iron doped calcium alginate biopolymer,* Journal of Radioanalytical and Nuclear Chemistry 274 (2007) 219-224

[55] Covaliu C., Matei C., Ianculescu A., Jitaru I., Berger D., *Fe_3O_4 and $CoFe_2O_4$ nanoparticles stabilized in sodium alginate polymer,* U.P.B. Scientific Bulletin, Series B 71 (2009) 1454-2331

[56] Ma H., Qi X., Maitani Y., Nagai T., *Preparation and characterization of superparamagnetic iron oxide nanoparticles stabilized by alginate,* International Journal of Pharmaceutics 333 (2007) 177-186

[57] Keng P., Lee S., Ha S., Hung Y., Ong S., *Removal of hazardous heavy metals from aqueous environment by low-cost adsorption materials,* Environmental Chemistry Letters 12 (2013) 15-25

[58] Vieira R., Meneghetti E., Baroni P., Guibal E., Cruz V., Caballero A., Castellon E., Beppu M., *Chromium removal on chitosan-based sorbents- An EXAFS/XANES investigation of mechanism,* Materials Chemistry and Physic 146 (2014) 412-417

[59] Yantasee W., Warner C., Sangvanich T., Addleman R., Carter T., Wiacek R., Fryxell G., Timchalk Ch. Warner M., *Removal of heavy metals from aqueous systems with thiol functionalized superparamagnetic nanoparticles,* Environmental Science and Technology 41 (2007) 5114-5119

[60] Liu J., zhao Z., Jiang G., *Coating Fe_3O_4 magnetic nanoparticles with humic acid for high efficient removal of heavy metals in water,* Environmental Science and Technology 42 (2008) 6949-6954

[61] Wang J., Zheng S., Shao Y., Liu J., Xu Z., Zhu D., *Amino-functionalized Fe_3O_4@SiO_2 core-shell magnetic nanomaterial as a novel adsorbent for aqueous heavy metals removal,* Journal of Colloid and Interface Science 349 (2010) 293-299

[62] Shishehbore M., Afkhami A., Bagheri H., *Salicylic acid functionalized silica-coated magnetite nanoparticles for solid phase extraction and preconcentration of some heavy metal ions from various real samples,* Chemistry Central Journal 5 (2011)

[63] Lin J., Wang L., *Comparison between linear and non-linear forms of pseudo-first-order and pseudo-second-order adsorption kinetic models for the removal of methylene blue by activated carbon,* Frontiers of environmental science & engineering in China 3 (2009) 320-324

[64] Soto M., Moure A., Dominguez H., Parajo J., *Recovery, concentration and purification of phenolic compounds by adsorption: A review,* Journal of food engineering 105 (2011) 1-27

[65] Ho Y., McKay G., *Pseudo-second order model for sorption processes,* Process Biochemistry 34 (1999) 451-465

[66] Mochamed Ch., *Applicability of some statistical tools to predict optimum adsorption isotherm after linear and non-linear regression analysis,* Journal of Hazardous Materials 153 (2008) 207-212

[67] Cao J., Wang Y., Yu J., Xia J., Zhang Ch., Yin D., Urs O., *Preparation and radiolabeling of surface-modified magnetic nanoparticles with rhenium-188 for magnetic targeted radiotherapy,* Journal of Magnetism and Magnetic Materials 277 (2004) 165-174

[66] Lu M., Liu Y., Hu X., Ben Y., Zeng X., Li T., Wang H., *Competitive adsorption of Cu(II) and Pb(II) ions from aqueous solutions by Ca-alginate immobilized activated carbon and Saccharomyces cerevisiae,* Journal of Central South University 20 (2013) 2478-2488 (od tego wszystkie w górę)

[67] Mürbe J., Rechtenbach A., Töpfer J., *Synthesis and physical characterization of magnetite nanoparticles for biomedical applications,* Materials Chemistry and Physics 110 (2008) 426-433

[68] Mahdavi M., Ahmad M., Haron M., Gharayebi Y., Shameli K., Nadi B., *Fabrication and characterization of SiO2/(3-aminopropyl)triethoxysilane- coated magnetite nanoparticles for Lead(II) removal from aqueous solution,* Journal of inorganic and organometallic polymers and materials 23 (2013) 599-607

[69] Shen M., Cai H., Wang X., Cao X., Li K., Wang S., Guo R., Zheng L., Zhang G., Shi X., *Facile one-pot preparation, surface functionalization, and toxicity assay of APTS-coated iron oxide nanoparticles,* Nanotechnology 23 (2012) 105601

[70] Goya G., Berquo T., Fonseca F., Morales M., *Static and dynamic magnetic properties of spherical magnetite nanoparticles,* Journal of Applied Physics 94 (2003) 3520-3528

[71] Salgueiro A., Daniel-da-Silva A., Girao A., Pinheiro P., Trindade T., *Unusual dye adsorption behavior of κ-carrageenan coated superparamagnetic nanopartices,* Chemical Engineering Journal 229 (2013) 276-284

[72] Hoppe J., Howell P., *Education in Chemistry,* 12 (1975) 12-15

Web sides:

[1] http://www.ph.utexas.edu/~laser/projects/shelled.html (16.07.2014)

[2] http://www.glantreo.com/otherparticles.php (16.07.2014)

ANNEX I

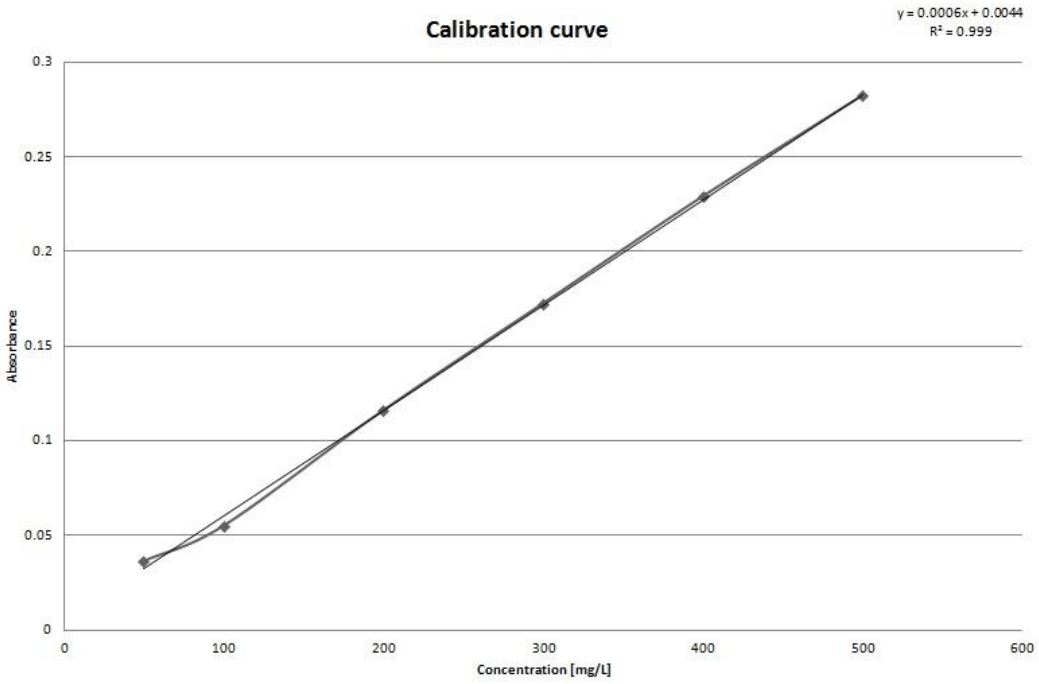

Figure 1. Calibration curve for [Cr(HY)(H_2O)]